IEEE Access
Multidisciplinary ⋮ Rapid Review ⋮ Open Access Journal

Received July 15, 2021, accepted July 27, 2021, date of publication July 28, 2021, date of current version August 12, 2021.

Digital Object Identifier 10.1109/ACCESS.2021.3101160

Analog Modeling of Fractional-Order Elements: A Classical Circuit Theory Approach

NEVEN MIJAT[1], (Life Member, IEEE), DRAZEN JURISIC[1], (Member, IEEE), AND GEORGE S. MOSCHYTZ[2], (Life Fellow, IEEE)

[1]Faculty of Electrical Engineering and Computing, University of Zagreb, 10000 Zagreb, Croatia
[2]Faculty of Engineering, Bar-Ilan University, Ramat Gan 52900, Israel

Corresponding author: Drazen Jurisic (drazen.jurisic@fer.hr)

This work was fully supported by the Croatian Science Foundation under the project IP-2016-06-1307 "Fractional Analog and Mixed Systems for Signal Processing".

ABSTRACT In this paper a comprehensive procedure for the analog modeling of Fractional-Order Elements (FOEs) is presented. Unlike most already proposed techniques, a standard approach from classical circuit theory is applied. It includes the realization of a system function by a mathematical approximation of the desired phase response, and the synthesis procedure for the realization of basic fractional-order (FO) one-port models as passive RC Cauer- and Foster-form canonical circuits. Based on the presented one-ports, simple realizations of two-port differentiator and integrator models are derived. Beside the description of the design procedure, illustrative examples, circuit diagrams, simulation results and practical realizations are presented.

INDEX TERMS Fractional-order element, fractional-order differentiator and integrator, fractional immittance, constant-phase element, approximation, synthesis, cauer one-port, foster one-port.

I. INTRODUCTION

There are many processes in technology and science which can be efficiently interpreted and analyzed using fractional-order (FO) derivatives and integrals. Fractional calculus which involves these operations, was developed several centuries ago, most of the time as a subject of purely mathematical interest. During the last century it became apparent that in many areas of science, various real systems can often be more accurately described by FO rather than by traditional integer-order (IO) models [1], [2]. This awareness has resulted in the increased development of fractional calculus applications in various fields of engineering and science. They include more efficient $PI^{\lambda}D^{\mu}$ controllers compared to conventional PID controllers [3]–[6], more precise lead/lag compensators [7], [8], a FO model that efficiently approximates the electroencephalographic measurement chain system [9], high-speed FO PLLs with broader capture range and bandwidth, lower phase error and shorter locking time [10], active-RC FO filters that allow for a fractional step in the stopband [11]–[15], FO resonators which can have infinite Q-factors [16], FO oscillators for very high or very low frequency signals [17], FO band-pass filters and resonators realized in integrated form allowing low frequency operation, huge inductance values and electronic tunability of order and other parameters [18], [19]. Besides, Westerlund has shown that capacitors with dielectric can only be modelled accurately with FO derivatives [20], because nature works with FO derivatives [21]. This property of capacitors directly affects modelling and measurement of supercapacitors, which can be fitted more precisely with an FO RC model than with a conventional RC model [22], [23]. Some authors have recently used FO mathematical models of capacitors and inductors in buck-boost and buck-converters, that allow a more accurate analysis of many properties, including the voltage gain of these converters [24], [25]. There are many other applications of FO models in the literature, including those in the digital domain [26]. A time and frequency analysis of electrical circuits with FO elements is presented in [27]. The application of FO derivatives in system theory and their relevance in representation of dynamical systems is shown in [28]. As a consequence of the raising applications, the development of new FO system models has become a challenging subject for many authors, particularly in the circuit theory field. A comprehensive overview of FO calculus and various developed models is given in [1] and [2].

The associate editor coordinating the review of this manuscript and approving it for publication was Xiaoli Luan.

The definition of FO derivatives and integrals requires the use of special mathematical functions, making the analysis of such systems difficult in the time domain. However, the Laplace transform can be applied to FO derivatives and integrals as well as to IO systems permitting the analysis and design of FO systems in the frequency domain with less difficulty than in the time domain.

As seen so far, one of the most intriguing problems for many authors dealing with this subject is to find a definition for the most suitable models of basic fractional-order elements (FOEs) that can be used as standard components of FO systems. Since the most convenient models are realized as electrical circuits, this problem necessarily involves circuit and systems theory methods for their design and realization. Note that some devices in the electrical engineering field, such as some forms of transmission lines, can be considered and analyzed as FO systems. Also, an important device used in audio signal processing is the well-known *pink noise filter*, whose transfer function is a typical model of an elementary FO function [29], [30]. References [31]–[33] provide an overview of how FOEs are realized in two approaches: 1) as a single component (e.g. fractal structures realized on silicon by micro-electronic process using MOS technology or in electrolyte, ionic gel-copper electrode based packaged FOEs, electrochemical, solid-state, metal-polymer composite based FOEs, ferro-electric polymer based FOEs, and so on.); 2) as a multi-component device (e.g. electrical circuits). It is not easy to produce a high-quality single-component device because such FOEs are cumbersome and unstable or have a narrow operating frequency bandwidth. Therefore, the second approach has been investigated recently [34]–[40] and in the past [26], [41]–[54], and is the subject of this paper.

In this paper we present a method for designing basic FO models as RC circuits using standard circuit-theory synthesis methods, which involve the approximation of a system function, and its realization as a final circuit. As expected, the circuit synthesis solution, if it exists, is not unique. Generally, there is an unlimited number of solutions and the designer has the possibility of choosing the one which best suits his application. We present solutions based on the realization of canonical one-port RC circuits for a given system function, as well as simple passive RC circuit models of FO integrator- and differentiator-derived two-port models.

The paper is structured as follows. In section II a definition and properties of the FO element are described. In section III two basic approximations, the maximally flat and the minimax approximation of the ideal system FO phase response, resulting in rational functions, are described. In section IV, an alternative approximation of the same phase response is derived, using the inverse rational function applied to the complementary constant phase. The frequency response comparison of the two basic approximations, maximally flat and minimax, shows the superiority of the minimax approximation and justifies its use in the rest of the paper. In section V, basic Foster and Cauer RC circuit models of FO one-port elements are presented and it is shown that for each value of constant phase at least eight different canonical one-ports can be realized. Based on the one-port circuits, simple realizations of basic two-port FO elements, e.g. integrators and differentiators are derived. In section VI the minimax approximation is compared to other approximations showing that in most cases it performs better than other known methods. In section VII a physical realization of FO one-port elements and measurement results are presented. A MATLAB program for the design of constant-phase elements, that was developed for this project is available on the internet and also from the authors (see [73]). Section VIII concludes this work.

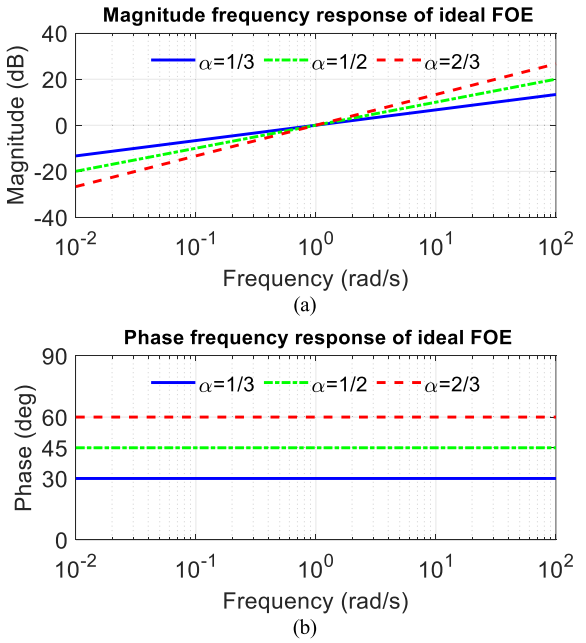

FIGURE 1. (a) Magnitude and (b) phase frequency response of ideal FOEs for three different values of order $0 < \alpha < 1$.

II. FRACTIONAL-ORDER ELEMENTS (FOEs)

A basic ideal FOE is defined by the system function in the complex frequency domain

$$F_i(s) = F_o \cdot s^{\alpha}, \tag{1}$$

where s is a complex frequency, F_o ($F_o > 0$) and fractional order α ($-1 < \alpha < 1$) are real constants, and subscript i denotes "ideal". Substituting $s = j\omega$ in (1) the frequency response is obtained as $F_i(j\omega) = F_o \cdot \omega^{\alpha} \cdot e^{j\alpha\cdot\pi/2}$, where

$$|F_i(j\omega)| = F_o \cdot \omega^{\alpha} \tag{2}$$

is the gain response and

$$\arg\left(F_i(j\omega)\right) = \varphi_i(\omega) = \alpha \cdot \frac{\pi}{2} = \varphi_i = \text{const.} \tag{3}$$

is the phase response of function (1). Both ideal frequency responses are shown in Fig. 1 for $\alpha = 1/3$, 1/2 and 2/3. Since the phase response is constant over the entire frequency range, an ideal FO element is often referred to as a *constant phase element* (CPE).

For modeling purposes, two kinds of basic circuit elements need to be defined: a basic one-port or two-terminal element characterized by its FO impedance or admittance, and a basic two-port or four-terminal element characterized by its transfer function,[1] e.g., FO integrator or differentiator. A one-port FO circuit element has an impedance $Z_i(s)$ or admittance $Y_i(s)$ which is identical to (1). The parameter α of FOE defines its character. If $F_i(s)$ is an impedance, then values $-1 < \alpha < 0$ designate the FOE as a FO *capacitance* (FOC), and values $0 < \alpha < 1$ as a FO *inductance* (FOI). If α attains the limiting values 1 or -1, $F_i(s)$ is the impedance of a conventional inductance or capacitance, respectively, and $\alpha = 0$ represents a pure resistance. A two-port FOE also has a transfer function identical to (1). The values $-1 < \alpha < 0$ designate an FO *integrator*, and values $0 < \alpha < 1$ an FO *differentiator*. For the two limits α: -1 or 1, it is a regular integrator or differentiator, and if $\alpha = 0$ it is an amplifier or an attenuator.

An important property of the ideal FOE is the dependence between the amplitude (2) and phase (3) response. They are directly related to the parameter α. In the Bode diagrams shown in Fig. 1, the amplitude response (with $F_o = 1$) is a straight line with slope equal to $20{\cdot}\alpha$[dB/decade] and the phase response is constant and equal to $\alpha \cdot \pi/2$ at all frequencies. In order to retain the similar unique dependence in the realized model, the phase and amplitude response of a model system function, which is a rational function of complex variable s, must obey Bode's integral relationship [55 pp. 312-314]. This condition limits the choice of possible rational functions either to *positive real* (PR) immittance functions of one-port FOE passive circuit models or to *minimum phase* (MP) transfer functions of a two-port FOE model. The common property of both function types is that all poles and zeros lie in the left half of the complex frequency s-plane.

III. APPROXIMATION OF IDEAL FO SYSTEM FUNCTION

The system function (1) of an ideal basic FO element is an irrational continuous function of a complex variable s, which cannot be realized by a finite circuit using conventional lumped elements. Therefore, a satisfactory approximation must be used. Our goal is to realize a lumped element electrical circuit as a good approximation of the ideal FOE within a given frequency range, and with minimal complexity. To do so, we need to produce an integer-order rational function, which is realizable as an electrical circuit with lumped elements and approximates $F_i(s)$ in the given frequency range with a tolerable error. So far, a variety of approximation procedures has been presented in the literature [26]–[54]. Most of them use an expansion of the system function (1), or an associated function, into an infinite series, or an infinite product of simple factors, which, after truncation, leads to a rational function of the complex variable s. The rational function is usually expanded into a partial fraction, or a continued fraction suitable for the realization of a passive immittance FOE model. Some procedures are complex, and in some cases the result can be an unrealizable rational function, e.g. a network with negative element values. Furthermore, most of the procedures are oriented to $\alpha = 1/2$ and do not give a general solution for any value of α.

In this paper we present a procedure for the realization of FOE models with any α within the limits $-1 < \alpha < 1$. We use the constant phase property of an ideal FOE in order to construct a rational system function with a nearly constant phase response in some prescribed frequency range for any phase between $-90°$ and $90°$. The maximum deviation of the phase function from the ideal value is controlled and can be specified in advance. Incidentally, some authors have dealt with the design of networks for the approximation of $45°$ constant phase for phase-splitting circuits in single sideband (SSB) transmission systems [56]–[60]. They were intended for the approximation of a $90°$ constant phase difference between the outputs of two all-pass networks. Basically, the approximation procedures can be applied to fractional-order modeling, as well. Here, we apply "maximally-flat" and "minimax" approximations to realize a rational function with a constant phase response of *any* value of φ_i ($-\pi/2 \leq \varphi_i \leq \pi/2$), e.g. of $\alpha{\cdot}90°$, where $-1 < \alpha < 1$.

We begin our analysis with the following constant-phase system function $F(s)$, or $F(j\omega)$, which we consider as an approximation of the ideal FOE system function (1), e.g.

$$F(s) \cong F_i(s) = F_o \cdot s^{\alpha}. \tag{4}$$

For convenience, the parameter F_o is denoted as the *value*, and α as the FO *parameter* of the modeled FOE. The value of F_o is identical to the module of $F_i(j\omega)$ at $\omega = 1$. Furthermore, the gain $|F(j\omega)|$ and the phase $\varphi(\omega) = \arg(F(j\omega))$ of the function $F(s)$ approximate the ideal function only in the limited frequency range within the defined upper and lower band-edge frequencies: ω_H and ω_L. Finally, since $\arg(F(j\omega))$ is an approximation of the ideal constant phase function $\arg(F_i(j\omega))$, the maximum allowed phase deviations need to be specified, as well. The network function $F(s)$ must be a *positive real* or *minimum phase* rational function of the form

$$F(s) = \frac{P(s)}{Q(s)}, \tag{5}$$

where $P(s)$ and $Q(s)$ are Hurwitz polynomials[2] [61], [62] with the following additional limitations on the roots of $P(s)$ and $Q(s)$. Simple roots on the imaginary axis are not allowed because their existence causes discontinuities of the phase response.[3] Only simple roots at the origin ($s = 0$) and at

[1] The transfer function can be any one of four functions: voltage transfer function, current transfer function, transfer impedance or transfer admittance.

[2] Here we use the most common definition of *Hurwitz polynomials* as those having all of the roots in the left half of the complex s plane, including simple roots on the imaginary axis. Polynomials having no roots on the imaginary axis are characterized as *strictly Hurwitz* polynomials.

[3] If $F(s)$ has simple poles or zeros on the imaginary axis a factor $(s^2 + \omega_v^2)$ corresponding to a conjugate pair of simple roots appears in its denominator or numerator. Consequently, the function $F(j\omega)$ will contain a factor $(\omega_v^2 - \omega^2)$. The frequency ω_v is the point where the phase function has a step discontinuity of π radians because $F(j\omega)$ changes the sign when ω changes from $\omega < \omega_v$ to $\omega > \omega_v$.

infinity ($s \to j\infty$) are allowed. The *positive real property* of a rational function is more restrictive than the *minimum phase* property. Beside the above condition on numerator and denominator, the positive real property also includes the following necessary condition involving its real part. *The real part of a positive real function $F(s)$ along the $j\omega$ axis (e.g.* $\mathrm{Re}[F(j\omega)]$*) is non-negative for all ω.* Therefore, if $F(s)$ is a positive real function, it satisfies the minimum phase property as well. In the sequel we use a positive real function $F(s)$ for the realization of both one-port circuit immittances and two-port circuit transfer functions.

If $F(s)$ has a constant phase, then the phase of its reciprocal $1/F(s)$ is also constant with the same absolute value, but with opposite sign. So if the approximation for $0 < \alpha < 1$ is known, then the approximation for negative α is also known.

For the purpose of the phase calculations that follow, it is convenient to obtain the following alternative form of (5)

$$F(s) = \frac{P(s)Q(-s)}{Q(s)Q(-s)} = \frac{S(s)}{Q(s)Q(-s)}. \tag{6}$$

The product $Q(s)Q(-s)$ in the denominator of (6) is an even order polynomial, with no effect on the overall phase. Consequently, the polynomial $S(s) = P(s)Q(-s)$ in the numerator of (6) has a phase function identical to the phase of the ratio $P(s)/Q(s)$. Thus, instead of seeking for a rational function with constant phase response, the problem is reduced to finding a polynomial with the same phase property.

The phase function $\varphi(\omega)$ is a transcendental function and it is more desirable in phase calculations to deal with a related rational function, such as

$$G(\omega) = \tan\varphi(\omega) = \left.\frac{S_O(s)}{jS_E(s)}\right|_{s=j\omega}, \tag{7}$$

where $S_E(\omega)$ and $S_O(\omega)$ are the even and odd parts of $S(s)$, respectively. In any frequency range in which the phase function $\varphi(\omega)$ approximates a constant, $G(\omega)$ also approximates a constant. *Therefore, we need to find a rational function* $G(\omega)$ which is nearly constant in a given frequency range. For synthesis purposes it is also convenient to work with a function of s rather than of $j\omega$, and after *analytic continuation* from the $j\omega$-axis into the s-plane, we define the corresponding function

$$T(s) = \frac{S_O(s)}{S_E(s)} = j\,G(\omega)|_{\omega=s/j}. \tag{8}$$

The function $G(\omega)$ is an odd rational function of ω, which can also be expressed as $G(\omega) = \tan(\varphi_P - \varphi_Q)$, where φ_P and φ_Q are respectively the arguments of the polynomials $P(s)$ in the numerator and $Q(s)$ in the denominator of $F(s)$ in (5) when $s = j\omega$. Since $G(\omega)$ must be nearly constant in the range $\omega_L \le \omega \le \omega_H$, as shown in Fig. 2, it is expected that at real frequencies ω it has no poles or zeros, because they would increase the deviations from a given constant value. The only exceptions are simple poles or zeros at $\omega = 0$ and $\omega = \infty$, meaning that the degree of the numerator and denominator differs by one. We assume first that $G(\omega) = 0$ at the frequency $\omega = 0$. The alternative case, when $G(\omega) = \infty$ at $\omega = 0$,

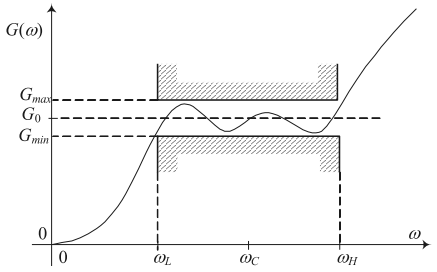

FIGURE 2. Approximation of a constant tan(φ) response.

is equivalent to $1/G(\omega) = 0$ at $\omega = 0$. The function $1/G(\omega)$ also approximates a constant in the same frequency range and is considered separately.

In general $G(\omega)$ has the form

$$G(\omega) = C_o \cdot \omega \frac{\left(\omega^2 + \omega_{o1}^2\right) \cdot \left(\omega^2 + \omega_{o2}^2\right) \cdots \left(\omega^2 + \omega_{om}^2\right)}{\left(\omega^2 + \omega_{p1}^2\right) \cdot \left(\omega^2 + \omega_{p2}^2\right) \cdots \left(\omega^2 + \omega_{pr}^2\right)}, \tag{9}$$

with $r - m = 0$ or 1, and C_o, ω_{oi} and ω_{pi}, are real constants. The highest degree of ω in (9) is the order of $G(\omega)$ e.g. the approximation order, and will be denoted as n. It is odd for $r - m = 0$ and even for $r - m = 1$. As an odd rational function of ω, $G(\omega)$ has an odd symmetry with respect to the origin. For our purpose we assume that $G(\omega)$ is also geometrically symmetrical with respect to the point $G(\omega_C)$, where $\omega_C = \sqrt{\omega_L \cdot \omega_H}$ is the center frequency of the approximation interval. We also assume that the frequency ω is normalized to ω_C, so that the center frequency is equal to 1. Furthermore we introduce the normalized function $G_o(\omega)$, defined as

$$G_o(\omega) = G(\omega)/G_\varphi \tag{10}$$

where $G_\varphi = \tan(\varphi_i)$ and φ_i is a specified constant phase. Clearly, the function $G_o(\omega)$ approximates $\tan(\varphi_i) = 1$ corresponding to $\varphi_i = \varphi_o = \pi/4$ or $\alpha = 1/2$. Finally, in order to enable comparisons between different approximation procedures, we define the lower and higher band-edge frequencies as $\omega_L = \sqrt{k}$ and $\omega_H = 1/\sqrt{k}$ and the maximum deviations of $G_o(\omega)$ in that range as $G_{\min} = \sqrt{k_1}$ and $G_{\max} = 1/\sqrt{k_1}$. The constants k and k_1 are real, positive and less than 1.

After $G_o(\omega)$ has been determined by an approximation procedure, a corresponding $F(s)$ can be found by standard circuit-theory procedures [61]. Using (8) we first find $T(s)$ and form $S(s)$ as a sum of its numerator and denominator, e.g.

$$S(s) = S_E(s) + S_O(s) = P(s) \cdot Q(-s). \tag{11}$$

In order to find $P(s)$ and $Q(-s)$ in (11) we calculate the roots of $S(s)$ by solving the equation

$$1 + T(s) = 0 \tag{12}$$

and present $S(s)$ in factored form. From (11) it is clear that all the roots that lie in the left-half plane belong to $P(s)$, while

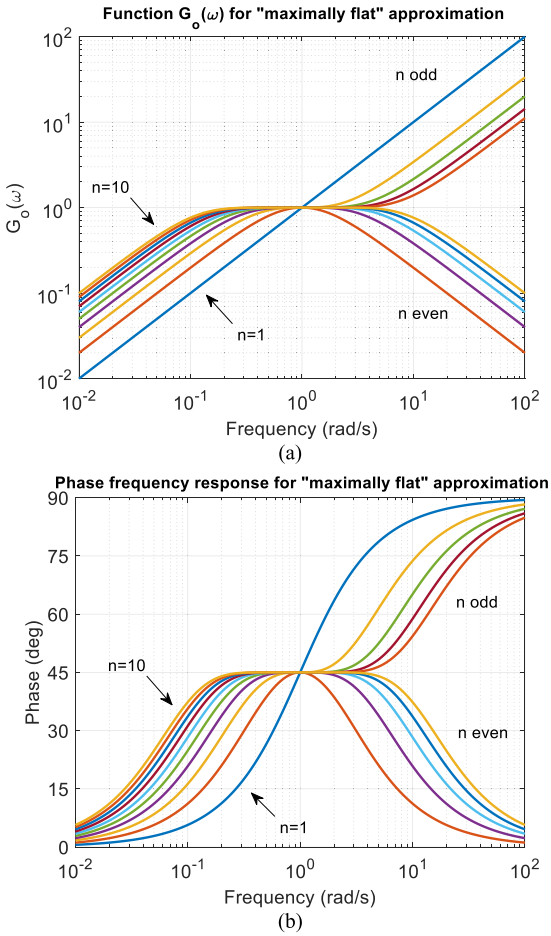

FIGURE 3. Maximally flat approximation of (a) $G_o(\omega) = \tan[\varphi(\omega)]$ and (b) corresponding constant phase response.

those in the right-half plane belong to $Q(-s)$. Finally, the desired system function is

$$F(s) = H \cdot \frac{P(s)}{Q(s)} = H \cdot \frac{\prod_i (s - s_{zi})}{\prod_j (s - s_{pj})}, \tag{13}$$

where s_{zi} are the zeros, s_{pi} the poles of $F(s)$ and H is an arbitrary positive constant. It is convenient to set the gain response equal to 1 at the center frequency 1, and the constant H should be calculated accordingly. The order N of the function $F(s)$ depends on the approximation order n. It is equal to $N = n/2$ if n is even, and $N = (n+1)/2$ if n is odd. In the following section we give a brief description of *maximally flat* and *minimax* approximations of the $\tan(\varphi)$ function.

A. MAXIMALLY FLAT APPROXIMATION OF TAN(φ) FUNCTION

A maximally flat approximation is an approximation of a function at one point. In our case we need to approximate a constant value $G_o(\omega) = 1$ at the normalized frequency $\omega = 1$. Its basic property is that as many derivatives as possible with respect to ω of the error function $1 - G_o(\omega)$ at $\omega = 1$ must be zero. As we deal with an n^{th}-order rational function or a polynomial, the first $n-1$ derivatives of that function must be zero at $\omega = 1$. The error function therefore has an n^{th}-order zero at the frequency $\omega = 1$, and can be generally defined as $1 - G_o(\omega) = K(1-\omega)^n / D(\omega^2)$, where $D(\omega^2)$ is an arbitrary even-order polynomial, and n is the approximation order. A simple calculation using the substitution $\omega = \tanh(x)$ yields $G_o(\omega)$ as

$$G_o(\omega) = \tanh\left[n \cdot a\tanh(\omega)\right] \tag{14}$$

and the function $T_o(s)$ corresponding to (14) is $T_o(s) = \tan[n \cdot \text{atan}(s)]$. The graphical representations of $G_o(\omega)$ and the corresponding phase functions for $n = 1, \ldots, 10$ for the approximation range of two decades, are shown in Fig. 3. The deviation of $G_o(\omega)$ from unity is zero at $\omega = 1$, and it increases as ω increases or decreases. The relation between the limits of the approximation band $G_{\min} = \sqrt{k_1}$ and $G_{\max} = 1/\sqrt{k_1}$ and the frequency range limits $\omega_L = \sqrt{k}$ and $\omega_H = 1/\sqrt{k}$ is given by (14) as $\sqrt{k_1} = \tanh\left[n \cdot a\tanh(\sqrt{k})\right]$. Therefore, they can be satisfied by the approximation of order n, derived as the smallest integer value obeying

$$n \geq \frac{a\tanh(\sqrt{k_1})}{a\tanh(\sqrt{k})}. \tag{15}$$

If the frequency limits are fixed, then the maximum deviation from unity decreases as the approximation order n increases. Also if the maximum deviation is fixed, then the approximation band increases as n increases. Each of the normalized curves in Fig. 3 has its maximum deviation from unity at the band edges.

The curves in Fig. 3 can also be used to find the appropriate approximation order when the maximum deviation, and the approximation frequency band, are given.

To derive the roots of the polynomial $S(s)$ in (11), we have to solve equation (12) for $T(s) = G_\varphi T_o(s)$. The values of s that satisfy (12) are

$$s_l = -\tan\left[\frac{\pi}{n}\left(\frac{1}{2} - \frac{\varphi_i}{\pi} + l\right)\right]; \quad l = 0, 1, \ldots, (n-1), \tag{16}$$

where φ_i is a specified positive constant phase in radians. All roots are real and lie either on the positive or negative part of the real axis in the s-plane. The negative roots belong to the polynomial $P(s)$; they are the zeros of the system function $F(s)$. The mirror images of the right half-plane roots belong to $Q(s)$; they are the poles of $F(s)$. The system function $F(s)$ has the form (13). Table 1 shows the poles, zeros, and system functions corresponding to the approximations shown in Fig. 3. It can be seen that the poles and zeros are all real, and alternate on the negative real axis in the complex frequency s-plane. The maximum phase deviations are shown in the second column of Table 1. They decrease as the approximation order increases.

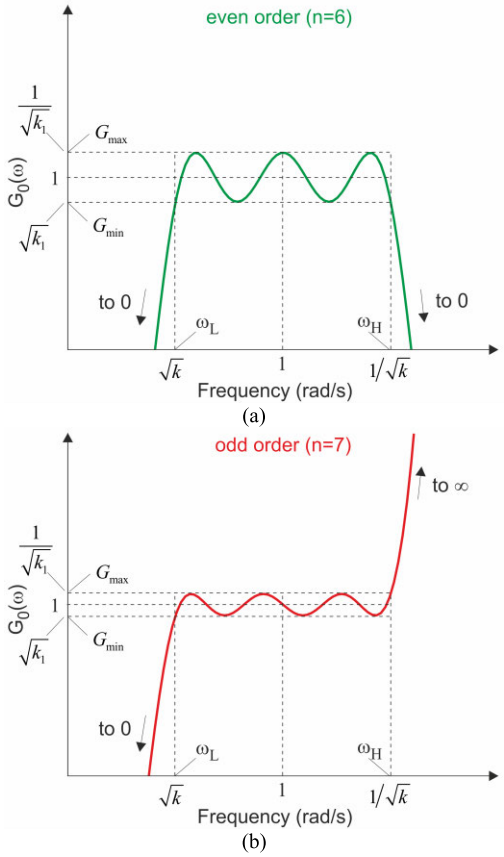

FIGURE 4. Minimax approximation of a constant phase response in the log-log plot for (a) even, and (b) odd approximation order n.

B. MINIMAX APPROXIMATION OF TAN(φ) FUNCTION

The minimax or Chebyshev approximation of $G_o(\omega)$ in a given frequency interval has the property that the maximum absolute value of the error function in the specified frequency interval is as small as possible. Consequently, the error function has equiripple behavior in the approximation range $\sqrt{k} \le \omega \le 1/\sqrt{k}$. $G_o(\omega)$ approximates $G_o = 1$ within the limits $\sqrt{k_1} \le G_o(\omega) \le 1/\sqrt{k_1}$. The behavior of $G_o(\omega)$ for an even ($n = 6$) and odd ($n = 7$) approximation order is shown in Fig. 4.

The approximation procedure of a function with equiripple variation within a given approximation band involves the use of Jacobi elliptic functions. Considering the above properties, the dependence between the function $G_o(\omega)$ and the frequency ω can be expressed in terms of two definite integrals, known as elliptic integrals of the first kind, namely

$$\int_0^{G_o/\sqrt{k_1}} \frac{dy}{\sqrt{(1-y^2)\left(1-k_1^2y^2\right)}} = \pm M_0 \int_0^{\omega/\sqrt{k}} \frac{dx}{\sqrt{(1-x^2)\left(1-k^2x^2\right)}}, \quad (17)$$

where x and y are the variables of integration and M_0 is a constant multiplier [56], [63], [64].

The solution of (17) can be written in the form of two parametric equations

$$G_o = \sqrt{k_1} \cdot \mathrm{sn}(Mu, k_1) \quad (18)$$

$$\omega = \sqrt{k} \cdot \mathrm{sn}(u, k), \quad (19)$$

where the new constant multiplier M is $M = M_0 \cdot (k/k_1)^{1/2}$. The function sn in (18) and (19) is the elliptic sine, i.e. one of the three basic Jacobi elliptic functions.[4] The constants k and k_1 are the modules of the above elliptic sn functions, and u is a parametric variable. The function $\mathrm{sn}(u, k)$ is doubly periodic with a real period $4K$ and an imaginary period $2K'$, where K and K' are the complete elliptic integrals of a modulus k and a complementary modulus $k' = \sqrt{1-k^2}$. The function $\mathrm{sn}(Mu, k_1)$ has a real period $4K_1$ and an imaginary period $2K_1'$. K_1 and K_1' are the complete elliptic integrals of modules k_1 and k_1' respectively. The detailed properties of the Jacobi elliptic functions are described elsewhere [63]–[65]. The function $T_o(s)$ follows from (18) and (19) by substituting $\omega = s/j$ and can be expressed as

$$T_o = \sqrt{k_1} \cdot \mathrm{sc}(Mu, k_1') \quad (20)$$

$$s = \sqrt{k} \cdot \mathrm{sc}(u, k'), \quad (21)$$

where the function sc is the elliptic tangent defined as the ratio between sn and cn functions with the complementary modules. The constant multiplier M is related to the periods of two sn functions by the relationship $M = K_1/K = nK_1'/K'$. This equation enables the evaluation of the approximation order n from a given k and k_1 as the smallest integer satisfying

$$n \ge \frac{K_1 \cdot K'}{K \cdot K_1'}. \quad (22)$$

The final step of the approximation design procedure is the derivation of the polynomial $S(s)$ in (11) and its roots. The roots can be found by solving equation (12) for $T(s)$, derived from (20) and (21). They are given by

$$s_i = -\sqrt{k} \cdot \mathrm{sc}\left(\left(v_\varphi + \frac{2iK'}{n}\right), k'\right); \quad i = 0, 1, \ldots, (n-1), \quad (23)$$

where v_φ is

$$v_\varphi = \frac{K'}{nK_1'} \mathrm{sn}^{-1}\left(1/\sqrt{1+G_\varphi^2 k_1}, k_1'\right), \quad (24)$$

where $G_\varphi = \tan(\varphi_i)$.

The function sn^{-1} is the inverse of the sn function, e.g. the incomplete elliptic integral of the first kind. All roots are real. Negative roots are the poles and the mirror images of the positive roots are the zeros of $F(s)$. The poles, the zeros, and the normalized system functions approximating $\varphi_i = 45°$ ($G_\varphi = 1$) within the two frequency decades, for $n = 1,\ldots,10$ are given in Table 2. The corresponding functions $G_o(\omega)$ and $\varphi(\omega)$ are shown in Fig. 5.

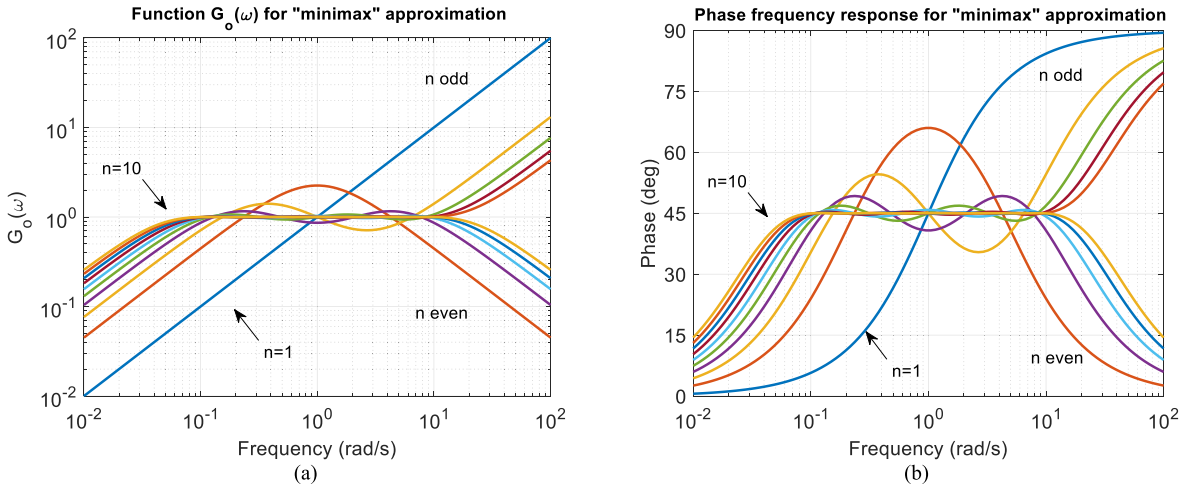

FIGURE 5. Minimax approximation within the bandwidth of two decades (a) $G_o(\omega) = \tan[\varphi(\omega)]$ and (b) corresponding constant phase response.

TABLE 1. Poles and zeros of F(s) - maximally flat approximation – Fig. 3.

n	$\Delta\varphi°$	Zeros	Poles	$F(s)$
3	28.7099°	-2.6795e-01 -3.7321e+00	-1.0000e+00	$\frac{0.353s^2+1.414s+0.353}{s+1}$
4	24.1384°	-1.9891e-01 -1.4966e+00	-5.0273e+00 -6.6818e-01	$\frac{3.359s^2+5.695s+1}{s^2+5.695s+3.359}$
5	20.1354°	-1.5838e-01 -1.0000e+00 -6.3138e+00	-1.9626e+00 -5.0953e-01	$\frac{0.2701s^3+2.018s^2+2.018s+0.2701}{s^2+2.472s+1}$
6	16.6984°	-1.3165e-01 -7.6733e-01 -2.4142e+00	-7.5958e+00 -1.3032e+00 -4.1421e-01	$\frac{4.1s^3+13.58s^2+9.313s+1}{s^3+9.313s^2+13.58s+4.1}$
7	13.7902°	-1.1267e-01 -6.2834e-01 -1.5915e+00 -8.8752e+00	-2.8578e+00 -1.0000e+00 -3.4992e-01	$\frac{0.2273s^4+2.548s^3+4.991s^2+2.548s+0.2273}{s^3+4.2078s^2+4.2078s+1}$
8	11.3549°	-9.8491e-02 -5.3451e-01 -1.2185e+00 -3.2966e+00	-1.0153e+01 -1.8709e+00 -8.2068e-01 -3.0335e-01	$\frac{4.729s^4+24.34s^3+32.76s^2+13.15s+1}{s^4+13.15s^3+32.76s^2+24.34s+4.729}$
9	9.3306°	-8.7489e-02 -4.6631e-01 -1.0000e+00 -2.1445e+00 -1.1430e+01	-3.7321e+00 -1.4281e+00 -7.0021e-01 -2.6795e-01	$\frac{0.2s^5+3.03s^4+9.25s^3+9.25s^2+3.03s+0.2}{s^4+6.128s^3+10.51s^2+6.128s+1}$
10	7.6564°	-7.8702e-02 -4.1421e-01 -8.5408e-01 -1.6319e+00 -4.1653e+00	-1.2706e+01 -2.4142e+00 -1.1708e+00 -6.1280e-01 -2.4008e-01	$\frac{5.28s^5+37.75s^4+79.57s^3+62.42s^2+17.14s+1}{s^5+17.14s^4+62.42s^3+79.57s^2+37.75s+5.28}$

TABLE 2. Poles and zeros of F(s) - minimax approximation for the bandwidth of two decades – Fig. 5.

n	$\Delta\varphi°$	Zeros	Poles	$F(s)$
3	9.5921°	-1.1731e-01 -8.5246e+00	-1.0000e+00	$\frac{0.164s^2+1.414s+0.164}{s+1}$
4	4.2417°	-8.2097e-02 -2.1375e+00	-1.2181e+01 -4.6785e-01	$\frac{5.699s^2+12.65s+1}{s^2+12.65s+5.699}$
5	1.8642°	-6.3566e-02 -1.0000e+00 -1.5732e+01	-3.4073e+00 -2.9349e-01	$\frac{0.166s^3+2.78s^2+2.78s+0.166}{s^2+3.7s+1}$
6	0.8183°	-5.2031e-02 -6.0340e-01 -4.7069e+00	-1.9219e+01 -1.6573e+00 -2.1245e-01	$\frac{6.77s^3+36.3s^2+21.1s+1}{s^3+21.1s^2+36.3s+6.77}$
7	0.3591°	-4.4116e-02 -4.1920e-01 -2.3855e+00 -2.2668e+01	-5.9988e+00 -1.0000e+000 -1.6670e-001	$\frac{0.137s^4+3.49s^3+8.99s^2+3.49s+0.137}{s^3+7.165s^2+7.165s+1}$
8	0.1576°	-3.8329e-02 -3.1757e-01 -1.4602e+00 -7.2719e+00	-2.6090e+01 -3.1489e+00 -6.8483e-01 -1.3752e-01	$\frac{7.737s^4+70.3s^3+106.3s^2+30.01s+1}{s^4+30.01s^3+106.3s^2+70.3s+7.737}$
9	0.0692°	-3.3905e-02 -2.5468e-01 -1.0000e+00 -3.9265e+00 -2.9494e+01	-8.5246e+00 -1.9632e+00 -5.0938e-01 -1.1731e-01	$\frac{0.122s^5+4.25s^4+19.5s^3+19.5s^2+4.25s+0.122}{s^4+11.11s^3+23.36s^2+11.11s+1}$
10	0.0303°	-3.0408e-02 -2.1245e-01 -7.3878e-01 -2.4930e+00 -9.7587e+00	-3.2886e+01 -4.7069e+00 -1.3536e+00 -4.0112e-01 -1.0247e-01	$\frac{8.612s^5+113.9s^4+314.7s^3+225.3s^2+39.45s+1}{s^5+39.45s^4+225.3s^3+314.7s^2+113.9s+8.612}$

It is known from filter theory that the minimax approximation performs much better than the maximally flat approximation. As can be seen from the $\Delta\varphi$ column in Table 1 and Table 2 the maximum phase deviation for the same order n is much smaller for the minimax approximation. This can also be illustrated by a simple example.

Example 1: Suppose we need to realize an approximation function $G_o(\omega)$ for the constant phase $\varphi = 45°$ with the maximum deviation of 1° in the frequency range between $\omega_L = 0.1$ rad/s and $\omega_H = 10$ rad/s. Then $\sqrt{k} = 0.1$ and $\sqrt{k_1} = \tan(44°) = 0.9657$. From (15) the approximation

[4]The basic three elliptic functions are: elliptic sine $\mathrm{sn}(u, k)$, elliptic cosine $\mathrm{cn}(u, k)$ and delta amplitude elliptic function $\mathrm{dn}(u, k)$.

order for the maximally flat approximation function is $n = 21$, and from (22) for the minimax approximation we get $n = 6$. Since the approximation order influences the complexity of the final circuit model, it is obvious that the minimax approximation is more efficient. Considering its obvious superiority, in the rest of the paper we use only the minimax approximation.

IV. APPROXIMATION WITH INVERSE FUNCTION G(ω)$^{-1}$

In the preceding section we assumed that $G(\omega) = 0$ at the frequency $\omega = 0$, and that the alternative case, for $G(\omega) = \infty$ at $\omega = 0$, is equivalent to $1/G(\omega) = 0$ at $\omega = 0$. The function $1/G(\omega)$ also approximates a constant in the same frequency range. However, if the approximated constant is not equal to 1 (e.g. $\varphi_i = 45°$), then it does not approximate the same constant. Let us denote $1/G(\omega)$ as $G'(\omega)$ and the corresponding system function as $F'(s)$. Since $G(\omega)$ is an approximation of $\tan(\varphi_i)$, then $G'(\omega)$ is obviously the approximation of $\cot(\varphi_i) = \tan(90° - \varphi_i)$. Therefore, the system function $F'(s)$, corresponding to $G'(\omega)$, has a phase which is complementary to the phase of $F(s)$ from (5), and is closely related to $F(s)$.

In this section we describe the procedure for deriving $F'(s)$ from the already known $F(s)$. The function $G'(\omega)$ has a pole at the origin, meaning that the system function has a phase equal to $\pi/2$ at $\omega = 0$.

We start with

$$jG'(\omega) = j\frac{1}{G(\omega)} = -\left.\frac{F_E(s)}{F_O(s)}\right|_{s=j\omega} = -\left.\frac{S_E(s)}{S_O(s)}\right|_{s=j\omega}. \quad (25)$$

The right-hand side of this equation indicates that the corresponding function $T'(s)$ is equal to

$$T'(s) = -\frac{1}{T(s)} = -\frac{F_E(s)}{F_O(s)} = -\frac{S_E(s)}{S_O(s)}. \quad (26)$$

Note that the function $T(s)$ in (8) is a ratio of the odd and even parts of $F(s)$ with an odd numerator and an even denominator. The function $T'(s)$ is also odd, but it has an even numerator and an odd denominator. This happens when the even and odd parts of the system function have a common factor which is cancelled by their division. Obviously, this common factor is an odd function of frequency. Since the system function is either *positive real* or *minimum phase* with a continuous phase in the entire frequency range, an odd denominator and even numerator of $T'(s)$ can only occur if a simple factor s is cancelled from its numerator and denominator [61]. So, the function $T'(s)$ in (26) can be written as

$$T'(s) = -\frac{s \cdot S_E(s)}{s \cdot S_O(s)}. \quad (27)$$

The corresponding polynomial $S'(s)$ is then

$$S'(s) = s \cdot (S_E(s) - S_O(s)) = P'(s) \cdot Q'(-s), \quad (28)$$

where $P'(s)$ and $Q'(s)$ are respectively the numerator and denominator polynomials of the new system function $F'(s)$.

The polynomial $S'(s)$ can also be written as

$$S'(s) = s \cdot S(-s) = s \cdot P(-s) \cdot Q(s). \quad (29)$$

The polynomial $P(s)$ belongs to the denominator of $F'(s)$ and $Q(s)$ to its numerator. The question is whether the factor s in (29), belongs to the numerator or the denominator of $F'(s)$. The functions $F(s)$ and $F'(s)$ are both positive real and must satisfy all necessary conditions of positive real functions. One of the properties that must be obeyed is that the real part of $F(j\omega)$ along the $j\omega$ axis is nonnegative, e.g. $\mathrm{Re}[F(j\omega)] \geq 0$ for all ω. As $\mathrm{Re}[F(j\omega)] = |F(j\omega)|\cos(\varphi(\omega))$, this also means that its phase is within the limits $-\pi/2 \leq \varphi \leq \pi/2$ for all ω. In the procedure above the function $F(s)$ has a positive phase $\varphi(\omega)$. The phase of its reciprocal $Q(s)/P(s)$ in $F'(s)$ is $-\varphi(\omega)$. If the factor s is a part of the numerator of $F'(s)$ then it contributes to the phase response with the constant amount of $\pi/2$ and the phase of $F'(s)$ is $\varphi' = \pi/2 - \varphi$. If it is in the denominator then the contribution is $-\pi/2$, and the phase of $F'(s)$ is $\varphi' = -\pi/2 - \varphi$. Since this exceeds the lower phase limit, *it violates the above PR property* and $F'(s)$ is no longer a PR function. Therefore, the only possibility is that

$$P'(s) = s \cdot Q(s) \quad (30)$$

and

$$Q'(s) = P(s). \quad (31)$$

The final form of $F'(s)$ is

$$F'(s) = H' \cdot s\frac{Q(s)}{P(s)} = \frac{s}{F(s)}. \quad (32)$$

H' is again a positive constant. $F'(s)$ is the reciprocal of the system function $F(s)$ multiplied by s. Its phase response is the complement to the phase of $F(s)$, and we denote it as $\varphi'(\omega) = \pi/2 - \varphi(\omega)$. Obviously, to approximate the originally given constant phase angle φ_i by $G'(\omega)$, we must calculate $G'_c(\omega)$ for the complementary angle $\varphi_{ic} = \pi/2 - \varphi_i$ [66], [67]. This is not necessary only if φ_i is equal to $\pi/4$, e.g. identical to its complement φ_{ic}. The point is that with this approximation procedure we obtain two different system functions for the same constant phase φ_i and we can choose which one better serves our purpose.

Example 2: The advantage of the minimax over the maximally flat approximation is shown in Fig. 6. The sixth order maximally flat and minimax approximations are applied for the realization of three different phase angles: $-30°$, $-45°$ and $-60°$ in the two-decade wide frequency range.

Both functions $G(\omega)$ and $G'(\omega)$[5] are implemented, and as a result four different approximation curves are displayed for each angle. The phase responses are normalized to the frequency $\omega_C = 1$, and the edge frequencies are $\omega_L = 0.1$ and $\omega_H = 10$. It can be seen at a glance that the maximally flat approximation curves have much larger maximum

[5]The approximations based on $G(\omega)$ are easily recognized as those with phase $0°$ at $\omega = 0$, while those with phase $-90°$ at $\omega = 0$ are based on $G'(\omega)$.

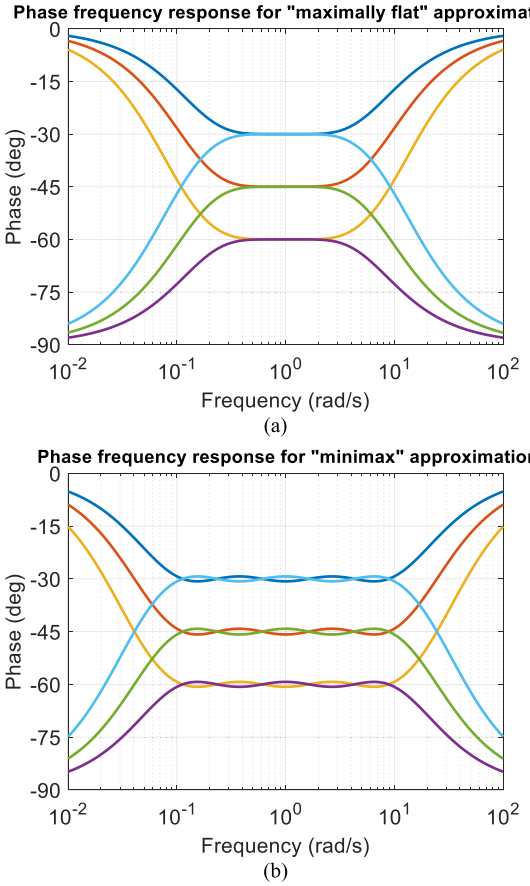

FIGURE 6. (a) Maximally flat and (b) minimax approximation of $-30°$, $-45°$ and $-60°$, constant phase response for the 6th order approximation.

phase variations than those of the minimax approximation. The maximally flat approximation has extreme variations at the edges of the approximation band, while the variations of the minimax approximation are distributed over the entire band. This, once again, confirms the superiority of the minimax approximation, and in the rest of the paper we use it for the realization of basic fractional-order elements. In classical circuit theory the minimax approximation is one of the basic approximation tools, particularly in electrical filter synthesis. As a mathematical tool it can be used wherever needed, as well as other approximation methods. However, in FO systems its application has never been worked out in a serious and comprehensive manner, and, as proposed in this paper, it is novel and may significantly improve the quality of FO circuit models.

The minimax approximation also performs very well compared to other known methods. As an illustration, we compare most of the referenced approximations to the minimax approximation of constant phase $\varphi = -45°$ in section VI.

V. CIRCUIT MODELS OF FO ELEMENTS

In this section we present synthesis procedures for the realization of basic one-port FOE models, as well as some simple passive realizations of two-port FOEs. Before we turn to the synthesis procedure of individual FOEs, let us examine the basic properties of the derived system functions. First, we can see that regardless of the approximation procedure used, the resulting system functions $F(s)$ and $F'(s)$ are rational functions of the complex frequency s with simple poles and zeros, which lie on the negative real axis in the complex s-plane. It is also apparent that the poles and zeros alternate with each other and the critical frequency nearest to or at the origin is a zero. The difference between the numerator and denominator order is 1 or 0. Any function which satisfies these properties is realizable as a driving point admittance of an RC one-port, or as a driving point impedance of an RL one-port.

The functions $F(s)$ and $F'(s)$ approximate a positive phase angle. For an approximation of a negative angle φ we have to use the reciprocal functions $1/F(s)$ or $1/F'(s)$. They are also rational functions of the complex frequency s with simple poles and zeros alternating on the negative real axis. However, the critical frequency nearest to or at the origin is a pole, and the difference between the numerator and the denominator order is 0, or -1. Any function satisfying these properties is realizable as a driving point admittance of an RL one-port or a driving point impedance of an RC one-port. Since we are dealing here with RC circuits rather than with RL circuits, we shall concentrate our attention on the functions that are suitable for the realization of RC impedances, e.g., $1/F(s)$ and $1/F'(s)$. Note that the phase function of RC impedance is always negative, and using a passive RC one-port, only a FO capacitance can be modeled. A FO inductance can only be modeled by an RL passive circuit. However, if we use active circuits, then an FO inductance can be realized as a combination of a passive RC circuit and an appropriate active element, as shown for example in [25], [35], and [37].

A. REALIZATION OF BASIC ONE-PORT FOE MODELS

There are four basic realization procedures for driving-point functions using RC networks: 1st and 2nd Foster and 1st and 2nd Cauer network forms [61], [62]. Foster forms are derived by the partial-fraction expansion (PFE) of a system function. The 1st Foster form follows from the PFE of a given RC impedance function, and the resulting circuit is a serial connection of parallel RC cells and possibly one resistor and/or one capacitor. The 2nd Foster form follows from the PFE of a corresponding RC admittance function, and the result is a parallel connection of serial RC cells and possibly one parallel resistor and/or one capacitor. Cauer networks are derived by the continued-fraction expansion (CFE) of a system function, e.g. the impedance function. The 1st Cauer network form corresponds to the CFE of a given RC impedance function about infinity and results in a ladder RC network with resistors in serial branches and capacitors in the parallel branches. For the 2nd Cauer network form the CFE is made about the origin and the resulting ladder circuit has capacitors in the serial branches and resistors in the parallel branches. The number of different realizations

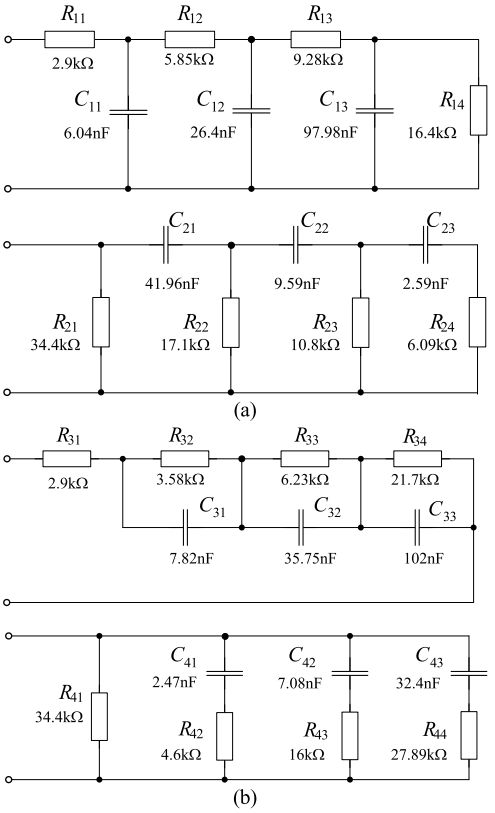

FIGURE 7. Realization of $\varphi = -30°$ CPE by (a) Cauer and (b) Foster canonical one-ports using the 6th-order approximation function G(ω).

TABLE 3. Normalized elements of Cauer and Foster RC one-ports with $Z(s) = F(s)$.

	i	1	2	3	4
1. Ca	C_{n1i} [F]	0.379	1.659	6.145	
	R_{n1i} [Ω]	0.2903	0.5847	0.928	1.641
2. Ca	C_{n2i} [F]	2.636	0.6027	0.1627	
	R_{n2i} [Ω]	3.444	1.7102	1.0775	0.609
1. Fo	C_{n3i} [F]	0.4913	2.246	6.43	
	R_{n3i} [Ω]	0.2903	0.3585	0.6232	2.172
2. Fo	C_{n4i} [F]	0.155	0.445	2.036	
	R_{n4i} [Ω]	3.444	0.4603	1.1605	2.789

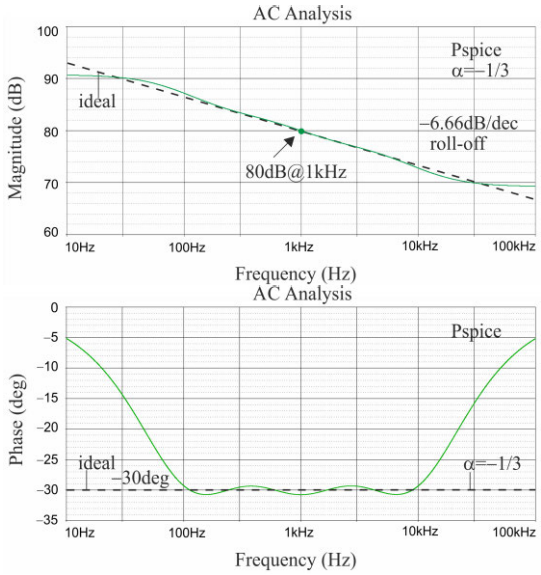

FIGURE 8. Frequency responses of Cauer and Foster canonical one-ports using the 6th-order G(ω) for approximation of $\varphi = -30°$ CPE.

can be increased by combining the various structures in the same synthesis procedure.

Example 3: As an illustration of the constant phase synthesis procedure, the angle $\varphi = -30°$ is approximated in a two-decade wide frequency range by a 6$^{\text{th}}$-order function $G(\omega)$ using the minimax approximation procedure. The resulting 3$^{\text{rd}}$-order system function is

$$F(s) = \frac{0.2903s^3 + 4.513s^2 + 6.463s + 1}{s^3 + 6.463s^2 + 4.513s + 0.2903}. \quad (33)$$

This is a normalized function with the center frequency $\omega_C = 1$ and the value $F_o = 1$. For some other central frequency and the value F_o the denormalization procedure must be applied either to $F(s)$ or to the final RC circuit. Here we choose the final circuit. It is actually the process of frequency and impedance scaling, e.g. transforming of each C_n and R_n into $C = C_n/(\omega_0 R_0)$ and $R = R_n R_0$, where R_0 is the normalization resistance and $\omega_0 = 2\pi f_0$ is the normalization frequency identical to the new central frequency. Cauer and Foster RC circuits are shown in Fig. 7. The normalized R and C values which follow from (33) are shown in Table 3. The denormalized element values for $R_0 = 10\text{k}\Omega$, and $f_0 = 10^3\text{Hz}$ are shown in Fig. 7. R_0 is identical to the new value F_o of the function (33).

The frequency response obtained by the Spice AC analysis is identical for all circuits in Fig. 7 and shown in Fig. 8. The gain at the central frequency f_0 is 80 dB, which is exactly the value of R_0 in dB. The phase response has an equiripple property in the approximation band, and the phase ripple is less than $\pm 1°$.

Example 4: Application of $G'(\omega)$ as the approximation function of the same angle $\varphi = -30°$ results in a new group of four RC circuits. For this purpose we first find the approximation function $G_c(\omega)$ for the complementary angle $\varphi_c = -60°$, and then take its reciprocal $G'_c(\omega)$, which approximates the angle $\varphi'_c = -\pi/2 - \varphi_c = -30°$. Using the procedure presented above, we obtain the new 4$^{\text{th}}$ order system function $F'_c(s)$ from $G'_c(\omega)$, i.e. the impedance $Z'_c(s)$ as

$$F'_c(s) = Z'_c(s) = \frac{14.74s^3 + 65.9s^2 + 31.7s + 1}{s^4 + 31.7s^3 + 65.9s^2 + 14.74s}. \quad (34)$$

Application of the Cauer and Foster synthesis procedure to (34) gives the four RC circuits shown in Fig. 9. The normalized element values are given in the Table 4, where the index c stands for *complementary*. The circuits in Fig. 9 are shown with the elements denormalized with respect to the same ω_0 and R_0 as above. The AC analysis results are identical for all circuits in Fig. 9 and are shown in Fig. 10.

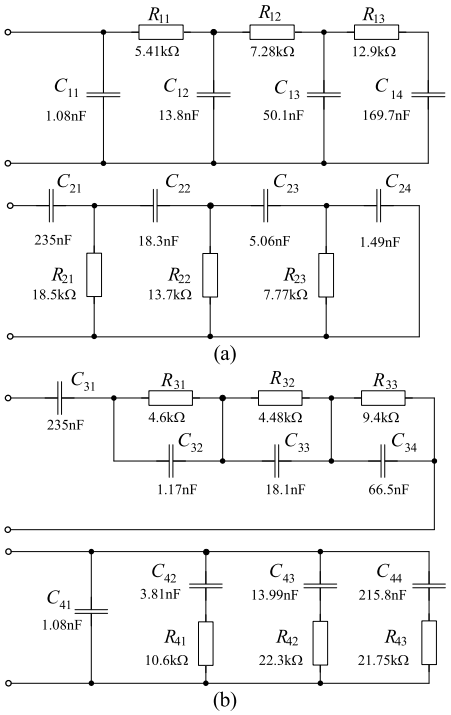

FIGURE 9. Realization of $\varphi = -30°$ CPE by (a) Cauer and (b) Foster canonical one-ports using the 6th-order approximation function G′(ω).

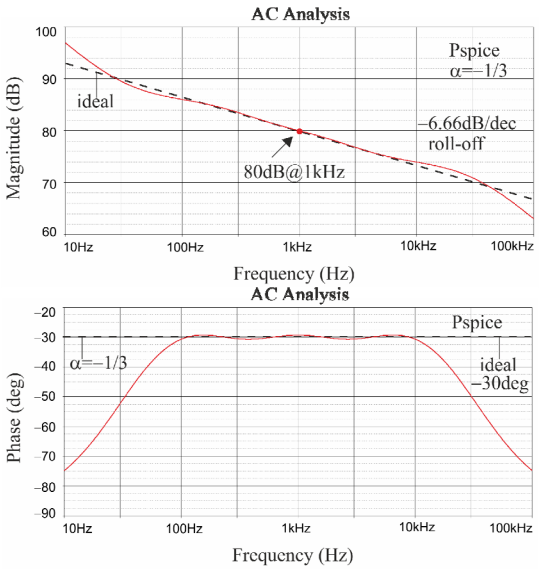

FIGURE 10. Frequency responses of Cauer and Foster canonical one-ports using 6th-order G′$_C$(ω) for approximation of $\varphi = -30°$ CPE.

B. REALIZATION OF BASIC TWO-PORT FOE MODELS

There are many different ways of realizing the two basic two-port FOE models, e.g. the FO integrator and the FO differentiator. In this section we present some voltage-mode and current-mode integrator and differentiator circuits realized as simple voltage or current dividers, derived from already known one-port models. The one-port circuits in Fig. 7 and Fig. 9 can be used for the realization of basic passive RC FO integrators and FO differentiators.

TABLE 4. Normalized elements of Cauer and Foster RC one-ports with $Z'_C(s) = F'_C(s)$.

	i	1	2	3	4
1. Ca	C_{nc1i} [F]	0.0678	0.868	3.145	10.66
	R_{nc1i} [Ω]	0.54	0.728	1.286	
2. Ca	C_{nc2i} [F]	14.74	1.15	0.318	0.0938
	R_{nc2i} [Ω]	1.847	1.374	0.775	
1. Fo	C_{nc3i} [F]	14.74	0.0736	1.137	4.178
	R_{nc3i} [Ω]	0.459	0.448	0.939	
2. Fo	C_{nc4i} [F]	0.0678	0.239	0.879	13.56
	R_{nc4i} [Ω]	1.064	2.232	2.175	

TABLE 5. Normalized elements of 2nd Cauer one-port created for $\varphi_C = -60°$.

	i	1	2	3	4
2.Ca	C_{n2i} [F]	3.444	1.7102	1.0775	0.609
	R_{n2i} [Ω]	2.636	0.6027	0.1627	

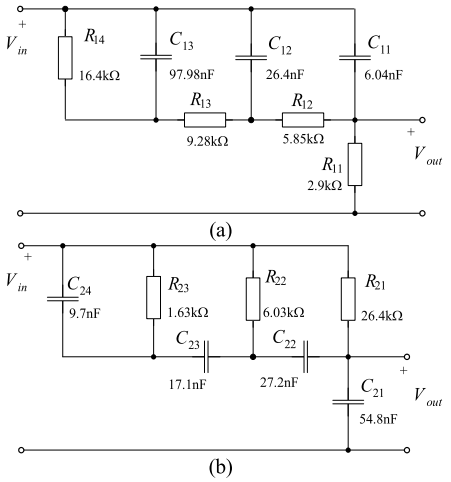

FIGURE 11. Realization of voltage mode passive RC FO (a) differentiator ($\varphi = 30°$) and (b) integrator ($\varphi = -30°$).

Example 5: The voltage-mode model for a FO differentiator and integrator can be realized as a voltage divider using any one-port model which has a single R or C serial element combined with the rest of the circuit. Using the one port models from Example 4, we can derive a differentiator and integrator having a constant phase of 30° and −30°, respectively.

A differentiator can be realized using either the Cauer first form or the Foster first form shown in Fig. 7. Choosing the Cauer first-form one-port, whose normalized element values are given in the first two rows (1.Ca) in Table 3, a differentiator is derived as the voltage divider circuit shown

in Fig. 11(a). The voltage divider transfer function is

$$F_{diff}(s) = \frac{V_{out}}{V_{in}} = \frac{R_{11}}{Z(s)}, \tag{35}$$

where $Z(s)$ is the one-port impedance. Since it has a constant phase of $-30°$, the phase of $F_{diff}(s)$ is constant and equal to $+30°$.

The realization of the integrator model requires a slightly different approach. It can be realized using the topology of the Cauer second form or the Foster first form from Fig. 9 to create the voltage divider in the same manner as for the differentiator. However, with the element values shown, the final integrator phase approximates the constant phase $\varphi = -60°$. Therefore, in order to realize a FO integrator with $\varphi = -30°$, we must use a suitable RC impedance with complementary constant phase equal to $-60°$. Let us use the second Cauer canonical one-port created for $\varphi_c = -60°$. Its normalized element values are shown in Table 5.

The derived integrator model has the form shown in Fig. 11(b), with the element values taken from Table 5, and denormalized to the frequency f_0 and the resistance R_0. Its transfer function is

$$F_{int}(s) = \frac{V_{out}}{V_{in}} = \frac{1}{sC_{21}Z_c(s)}, \tag{36}$$

where $Z_c(s)$ is the FO impedance with the complementary phase $-60°$. The phase of $F_{int}(s)$ is equal to the negative phase of the product in the denominator of (36), e.g. $\varphi = -(90° + \varphi_c) = -30°$.

It is also possible to derive the integrator from already known differentiator circuits in a much simpler way. The ideal integrator transfer function can be considered to be derived from the differentiator transfer function using the substitution $s \rightarrow 1/s$.[6] The same can be applied to their circuit-model transfer functions. Moreover, using the RC-CR transformation we can derive the elements of the integrator circuit directly from the differentiator model [68]. The RC-CR transformation is the procedure of creating a new RC circuit by replacing each capacitor C_i in a given circuit by a resistor equal to $1/C_i$ and each resistor R_i by a capacitor equal to $1/R_i$. The procedure is applied to the circuits with normalized element values. If we deal with voltage or current transfer functions of two-port circuits $F_a(s)$ and $F_b(s)$, then they are related as $F_a(s) = F_b(1/s)$. Since we already know that the normalized differentiator and integrator transfer functions are related as

$$F_{int}(s) = F_{diff}(1/s) \tag{37}$$

it is obvious that the RC-CR transformation applied to a differentiator circuit results in an integrator circuit.

[6]The frequency transformation $s \rightarrow 1/s$ is common in filter design, as a procedure for transforming a low-pass to a high-pass filter. When applied to a positive real function $F(s)$ it results in a function $F(1/s)$ which is also positive real. This follows from the property of the composition of two PR functions, namely if two functions $F_1(s)$ and $F_2(s)$ are PR, then their composition $F_1(F_2(s))$ is also PR [61]. Therefore, this transformation changes neither the PR property nor the stability property of the function.

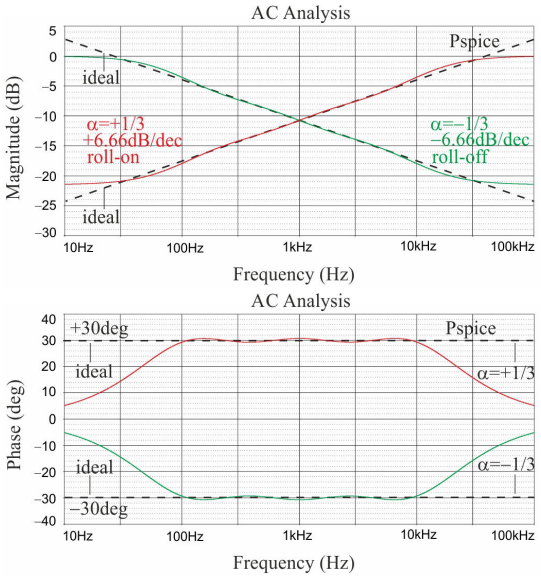

FIGURE 12. Amplitude and phase response of passive RC FO differentiator and integrator from Fig. 11.

TABLE 6. Normalized elements of 1st Cauer one-port created for $\varphi_c = -60°$.

	i	1	2	3	4
1.Ca	C_{n2i} [F]	0.2903	0.585	0.928	1.641
	R_{n2i} [Ω]	0.379	1.659	6.145	

This can easily be verified by inspecting the element values of the differentiator two-port in the first two rows of Table 3 and the elements of the integrator two-port in Table 5. The AC analysis for the two circuits in Fig. 11 is shown in Fig. 12. Both circuits have a drawback which is common to all passive RC two-port circuit synthesis procedures, namely that the resulting value of F_o of the FOE model generally differs from the one given in advance. In the differentiator it is limited by the resistor voltage divider ratio remaining after removing the capacitors, and in the integrator by a capacitance voltage divider ratio remaining after removing the resistors. In each case F_o is decreased by the corresponding voltage divider. Thus, in order to obtain the exact value of F_o, an active device such as a voltage amplifier can be used to obtain the desired value of F_o.

The current-mode models of an FO differentiator and integrator can be realized with any one-port model which has a single R or C parallel element combined with the rest of the circuit. Again, we use the one-port models from Example 4 to derive a differentiator and integrator with the constant phase 30° and −30°, respectively.

The integrator can be realized using either the Cauer second form, or the Foster second form from Fig. 7. Choosing the Cauer second-form one-port, with the normalized element values in the third and fourth rows (2.Ca) in Table 4, an integrator is derived as a current divider circuit shown in Fig. 13(a). The output current is the current through R_{21}

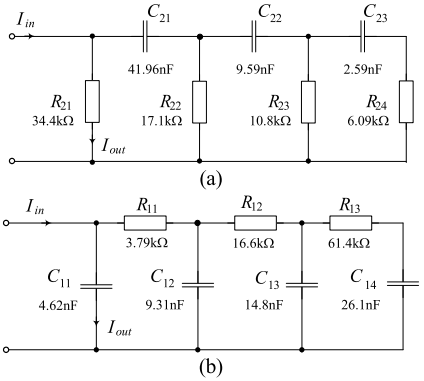

FIGURE 13. Realization of current mode passive RC FO (a) integrator ($\varphi = -30°$) and (b) differentiator ($\varphi = 30°$).

and the element values are denormalized with respect to the same frequency and resistor as above. The transfer function of the current divider is

$$F_{int}(s) = \frac{I_{out}}{I_{in}} = \frac{I_{R21}}{I_{in}} = \frac{Z(s)}{R_{21}}. \tag{38}$$

The current-mode differentiator can be realized using the topology of the Cauer first form or the Foster second-form one-port from Fig. 9 to create the current divider circuit shown in Fig. 13(b). As before, in order to realize an FO differentiator with $\varphi = 30°$, a suitable RC impedance with complementary constant phase equal to $-60°$ must be used. Let us use the first Cauer canonical one-port topology shown in Fig. 9, created for constant phase $-60°$. The normalized element values of this one-port are shown in Table 6. The same element values can be obtained by applying the RC-CR transform to the normalized element values of the first Cauer one-port topology in Fig. 7. Taking the current through C_{11} as the output current, the transfer function is obtained as

$$F_{diff}(s) = \frac{I_{out}}{I_{in}} = \frac{I_{C11}}{I_{in}} = sC_{11}Z_c(s). \tag{39}$$

The frequency response of both circuits is identical to the corresponding response of the voltage-mode circuits in Fig. 12. The current-mode two-ports suffer from the same drawback as the voltage-mode circuits, namely that the value F_o of the FOE model is also smaller than the desired value. In the integrator it is limited by the resistor current divider ratio remaining after removing the capacitors, and in the differentiator by a capacitor current divider ratio remaining after removing the resistors. Here again it can be corrected using a corresponding current amplifier.

VI. A COMPARISON OF THE MINIMAX APPROXIMATION TO OTHER APPROXIMATION METHODS

In order to compare the different approximation methods, we define 6 design parameters needed in the design of non-ideal FOEs. They are: the fractional order α (or equivalently the approximate phase angle φ_i), the value F_o in (1), the frequency limits of the constant-phase bandwidth (CPB) ω_L and ω_H (or equivalently the specified bandwidth $BW = \omega_H/\omega_L$ and the central frequency ω_c), the phase deviation $\Delta\varphi°$ (or $G_{\max}/G_{\min}$) representing the specified maximum allowable phase variation within the CPB limits as shown in Fig. 2, and the function order N (or approximation order n).[7] The approximation methods used for the comparison are presented in chronological order. The system approximation functions obtained by analytical methods are calculated using the procedures presented in the literature [34], [43], [45], [46], [49]–[52]. The other ones, derived by numerical optimization methods, are calculated using the results presented in the [38]–[40]. The approximation functions are normalized in order to make their magnitudes equal to unity at the unity frequency.

A. APPROXIMATION METHODS USED FOR COMPARISON

1) CARLSON-HALIJAK (1964) [41]

The earliest iterative procedure was by Carlson and Halijak [41] who used the order α as an input parameter. In a regular Newton process, the Carlson Halijak method realizes an approximation of discrete constant values of phase φ_i corresponding to $\alpha = 1/2$, 1/3, etc. Each iteration results in a system function whose order depends on α and the number of iterations. For example, for $\varphi_i = -45°$ after two iterations, the 4th–order function obtained is

$$F_{CH}(s) = \frac{s^4 + 36s^3 + 126s^2 + 84s + 9}{9s^4 + 84s^3 + 126s^2 + 36s + 1}. \tag{40a}$$

The third iteration results in a 13th–order function. Another value of the fractional exponent, for example $\alpha = -1/3$ ($\varphi_i = -30°$), results in a 1st, 2nd and 3rd iteration function of 1st, 5th and 21st order N, respectively. The method is unpredictable regarding the phase variation and the bandwidth. Some system functions obtained by this procedure can be realized only by RLC circuits, and not by circuits with two kinds of elements.

2) OLDHAM-ZOSKI [49]

The method presented by Oldham and Zoski [49] has the fractional order α and two time constants t_M and t_m, corresponding to the frequency limits ω_L and ω_H respectively, as initial design parameters. The procedure uses a 1st Foster form RC-network resulting in the series connection of N parallel RC branches and one resistor referred to as a "domino-ladder network". The resistor and capacitor values form a geometric progression depending on the value α. Apart from the calculated RC cells, two additional RC cells are required to optimize the phase response $\varphi(\omega)$,[8] thereby increasing the system function order by 2. In our example, we chose $\alpha = 1/2$, $t_M = 10$, $t_m = 0.1$ (2 frequency decades), $R_0C_0 = 25.4$, the progression ratio of resistors and capacitors $g = G = 2.573$ and the total order $N = 6$. The final network

[7] Note that the parameter F_o has no influence on the system function phase response. It can be used for the normalization or denormalization of the function magnitude.

[8] A similar process is used in some other referenced approximations.

is a series connection of six parallel RC branches and one resistor. The normalized impedance function obtained from the network is given by (40b), as shown at the bottom of the page.

3) CHAREF *et al.* [50]

The method of Charef *et al.* [50] is used for the approximation of the magnitude function $20{\cdot}\log|F_i(\mathrm{j}\omega)|$ and uses the maximum deviation of the magnitude function as a starting parameter. A system function with a single fractional-order pole and the fractional order α ($0 < \alpha < 1$) is approximated by a rational function with logarithmically spaced real poles and zeros alternating on the negative real axis in the s-plane. The input data is: the order α, the maximum magnitude deviation y in dB from $-20\alpha{\cdot}$dB/dec, the frequency limits ω_L (defined as the relaxation time constant) and ω_H. In our example we use $\alpha = 1/2$, $y = 2$dB, $\omega_L = 1.578{\cdot}10^{-2}$ and $\omega_H = 1.578{\cdot}10^{2}$, e.g. four frequency decades with a unity center frequency. The order of the obtained system function is $N = 5$, and the normalized system function is

$$Z_{Cha}(s) = \frac{1.0364s^4+19.33s^3+49.17s^2+19s+1}{0.1323s^5+6.2s^4+39.76s^3+39.4s^2+6.038s+0.127} \tag{40c}$$

4) MATSUDA-FUJII [46], [51]

The approximation procedure of Matsuda and Fujii is performed by expanding the function $F_i(s)$ with $\alpha = 1/2$ into a continued fraction expansion (CPE) and fitting it into a set of $n + 1$ logarithmically spaced points in the range $(s_\mathrm{L}, s_\mathrm{H})$, where n is the approximation order. The CPE is truncated after the n^{th} term. The input parameters are the order α and the frequency band limits. We chose $f(s) = s^{-1/2}$, $s_\mathrm{L} = 0.1$, $s_\mathrm{H} = 10$ (2 frequency decades) and $n = 8$. The result is a 4^{th}-order system function given by

$$Z_{Ma}(s) = \frac{0.0855s^4+4.8765s^3+20.838s^2+12.9955s+1}{s^4+12.9955s^3+20.838s^2+4.8765s+0.0855} \tag{40d}$$

5) OUSTALOUP *et al.* [46], [52]

This method is based on the approximation of s^α by a product of N bilinear rational functions using the fractional order α, and the frequency limits ω_H and ω_L as the initial parameters. The poles and zeros of the system function are logarithmically spaced, depending on α and the bandwidth. This procedure generates *only odd-order approximations* equal to $N = 2k + 1$ ($k = 1,2,\ldots$). If we choose $\alpha = -1/2$, $k = 2$, $\omega_L = 10^{-2}$ and $\omega_H = 10^2$ (4 decades) we get the impedance function

$$Z_{Oust}(s) = \frac{s^5+74.97s^4+768.5s^3+1218s^2+298.5s+10}{10s^5+298.5s^4+1218s^3+768.5s^2+74.97s+1} \tag{40e}$$

Note that the Oustaloup approximation is usually designed for a wider frequency band, e.g. $\omega_L/10$ and $10\omega_H$, instead of ω_L and ω_H [46]. Therefore (40e) is efficient within a bandwidth of 2 decades. Xue *et al.* [53] presented a modified Oustaloup approximation method for FO systems to reduce fitting problems at high and low frequencies, and better results were obtained. However, it resulted in a higher order and is not considered for a comparison here.

6) KRISHNA-REDDY [26], [54]

This procedure begins with the Continued Fractions Expansion (CFE) of the expression $(1 + x)^\alpha$ [69 p. 101]. By inserting $x = s - 1$ into it and truncating after a certain number of terms, the rational approximations for s^α obtained up to the 5^{th} order are shown in [26]. For $\alpha = -1/2$ in this work the 5^{th} order impedance is

$$F_{KR}(s) = \frac{s^5+55s^4+330s^3+462s^2+165s+11}{11s^5+165s^4+462s^3+330s^2+55s+1} \tag{40f}$$

Note that Matsuda and Fujii [51], Oustaloup *et al.* [52], Krishna and Reddy [54] do not require a specification of the value for the maximum phase deviation $\Delta\varphi^\circ$.

7) VALSA-VLACH [43]

Valsa and Vlach [43] proposed a method using $\Delta\varphi^\circ$ as the specification (together with the fractional order α and the frequency limits $\omega_{\max}$ and $\omega_{\min}$). The procedure is based on the Foster second form RC network. R and C values are calculated as a geometric progressions depending on the value of α and $\Delta\varphi$, thereby improving the previous idea of Machado [42]. Each element value is calculated from the previous step using a *recursive algorithm* (RA). In our example we chose $\alpha = -0.5$, $\Delta\varphi = 1^\circ$, $\omega_{\max}/\omega_{\min} = 10^2$, $R_1 = 1$, $C_1 = 23.8$ and obtained $\omega_{\min} = 1/(R_1C_1) = 0.042$. The normalized network impedance is equal to

$$Z_{Valsa}(s) = \frac{13.52s^4+373.5s^3+1103.9s^2+381.6s+14.11}{s^5+97.8s^4+856.8s^3+866.1s^2+101s+1.06} \tag{40g}$$

8) EL-KHAZALI [45]

The El-Khazali procedure extends the idea of the product of bilinear sections in the algorithm of Oustaloup to the product of biquadratic sections. Consequently, it provides *only even-order approximations*. The design depends solely on the fractional order α. Following the procedure in [45]

$$Z_{Old}(s) = \frac{0.74s^6+12.6s^5+385.7s^4+1735.7s^3+1163.3s^2+115.7s+1.57}{s^6+89s^5+1039.5s^4+1798s^3+467.1s^2+17.97s+0.090758} \tag{40b}$$

for the approximation of the system function as a product of biquadratic functions for $F_i(s)$ with $\alpha = 0.5$, we realized the 4th-order impedance function

$$Z_{ElKha}(s) = \frac{1.457s^4+86.27s^3+536.8s^2+300.6s+17.7}{17.7s^4+300.6s^3+536.8s^2+86.27s+1.457} \tag{40h}$$

The following three methods use numerical optimization procedures for the approximation of the FOE system function. They are: Flower Pollination Algorithm (FPA) [38], Cuckoo Search Optimizer (CS) [39] and Genetic Algorithm (GA) [40].

9) ABDEL-ATY *et al.* [38]

FPA and CS are based on the semi-analytical approach to the s^α approximation problem in [38]. The algorithm searches for the optimum coefficients (k_i, τ_i) in the sum of n first-order rational functions in the form $f_i(s) = k_i/(s + 1/\tau_i)$ $i = 1, 2, \ldots, n$ within the given frequency range (f_L, f_H), divided into n logarithmically equal sections in the selected number of points/decade. The cost function to be minimized is defined as the weighted sum of the absolute relative magnitude and phase errors. The final rational function is used for the realization of a Foster 2nd-form admittance, or as a transfer function using amplifiers to sum the output signals from individual RC cells. For comparison purposes, we use the example in [38] where the FPA is performed over 6 decades (f_L = 1Hz to f_H = 1MHz) having $n = 6$ equal frequency intervals within (f_L, f_H) and 100 points/decade for $\alpha = 0.5$. The resulting 6th-order normalized impedance function is (40i), as shown at the bottom of the next page.

10) YOUSRI *et al.* [39]

The Cuckoo Search optimizer (CS) performs similarly to the FPA, but using a different algorithm, so that for $\alpha = 0.5$ a different set of optimal coefficients (k_i, τ_i) is obtained. For comparison, we use the example in [39] where the CS optimization is performed through 6 decades (f_L = 1Hz to f_H = 1MHz) with a CS technique giving 6 pairs of (k_i, τ_i). The normalized 6th-order impedance approximation function of s^α is (40j), as shown at the bottom of the next page.

11) KARTCI *et al.* [40]

The Genetic Algorithm (GA) in [40] is used for the optimization of the phase and/or magnitude response of an RC or RL network in the given frequency range. We use the design of the Foster-II RC network performed over 4 decades (f_L = 100Hz to f_H = 1MHz) with 12 elements (R_0, C_0 to R_5, C_5), calculated for $\alpha = -0.5$. The final 5th-order normalized impedance function is

$$Z_{GA}(s) = \frac{0.043s^5+10.6s^4+181.3s^3+300s^2+49.4s+0.75}{s^5+58.13s^4+309.1s^3+161.9s^2+8.24s+0.0302} \tag{40k}$$

12) ADHIKARY *et al.* [34]

The procedure by Adhikary *et al.* [34] is used for the design of the Foster structure with the specified phase band variation $\Delta\varphi°$, fractional order α, frequency band limits (f_L, f_H), and value F_o. As a result, the RC component values of the modified Foster I and II form are derived. This approximation process is similar to those by Oldham and Valsa. In our example we start with $\alpha = 0.5$, $\Delta\varphi = 3°$, $f_L = 1$, $f_H = 10^3$ and $F_o = 1$. The normalized impedance function calculated from the circuit element values is

$$Z_{Adhk}(s) = \frac{0.045s^5+18.42s^4+931s^3+3125s^2+707.5s+10.3}{s^5+197.5s^4+2512s^3+2191s^2+131s+0.504} \tag{40l}$$

As can be seen, some methods have the final circuit with the element values as a result, while others have the system function $F(s)$. The latter approach is advantageous because, in the next step, we can calculate the variety of RC networks from the calculated $F(s)$.

B. A COMPARISON OF APPROXIMATION METHODS

The minimax procedure uses all 6 basic input parameters α, F_o, ω_L, ω_H, n, and $\Delta\varphi°$ defined in the beginning of this section for the design of the non-ideal Fractional-Order Elements (FOEs). In this method the phase deviation $\Delta\varphi°$, the frequency bandwidth BW and the approximation order n are mutually related, and only two of them need be given in advance, after which the third is calculated. In order to enable a meaningful comparison, the minimax approximation impedance functions that realize $\alpha = -0.5$, should have the same approximation order n and bandwidth BW as the functions given in (40). Since those functions have different orders and bandwidths, they are divided into five groups having the same order and bandwidth. They are compared to the minimax FO impedances with the order and bandwidth as close as possible to the other compared functions. The results are presented for each group separately in Fig. 14(a)-(e). The approximation impedances with BW = 10^3 and $n = 10$ are compared to the minimax function in Fig. 14(a).

$$Z_{Mmx_a}(s) = \frac{0.076s^5+6.4s^4+57.3s^3+87.9s^2+24.2s+1}{s^5+24.2s^4+87.9s^3+57.3s^2+6.4s+0.076} \tag{41a}$$

In Fig. 14(b) the approximation impedances with BW = 10^3 and $n = 8$ are compared to the minimax function

$$Z_{Mmx_b}(s) = \frac{0.0845s^4+5.39s^3+27.05s^2+15.89s+1}{s^4+15.89s^3+27.05s^2+5.39s+0.0845} \tag{41b}$$

In Fig. 14(c) the approximation impedance with BW = $4{\cdot}10^2$ and $n = 12$ is compared to the minimax

function

$$Z_{Mmx_c}(s) = \frac{0.083s^6+6.37s^5+69.7s^4+186s^3+134s^2+25.5s+1}{s^6+25.5s^5+134s^4+186s^3+69.7s^2+6.37s+0.083} \quad (41c)$$

In Fig. 14(d) the approximation impedances with BW = $6.26{\cdot}10^5$ and $n = 11$ are compared to the minimax function (41d), as shown at the bottom of the next page.

In Fig. 14(e) the approximation impedance with BW = $1.723{\cdot}10^4$, and $n = 10$, is compared to the minimax function

$$Z_{Mmx_e}(s) = \frac{0.043s^5+10.37s^4+176.1s^3+308.4s^2+57.1s+1}{s^5+57.1s^4+308.4s^3+176.1s^2+10.37s+0.043} \quad (41e)$$

Apart from the graphical comparison, the maximum phase deviation of each curve within the bandwidth $\omega_H \le \omega \le \omega_L$ is calculated numerically using the following measure

$$\Delta\varphi_{\max} = \max_{\omega_L \le \omega \le \omega_H} |\varphi_i - \arg(Z(j\omega))| \quad (42)$$

The values of $\Delta\varphi_{\max}$ obtained in degrees are shown in Fig. 14 within the brackets.

As can be seen, the minimax approximation has an equiripple property within the approximation band and generally the smaller deviation, even though it has a somewhat broader frequency band than some of the other approximations. It's maximal deviation from 45° is less than 0.3° for a 5th-order system function (Fig. 14a) and less than 1° for a 4th-order function (Fig. 14b). The phase deviations of the minimax approximation are uniformly distributed along the approximation band, while most of the other approximations have small phase deviations in the neighborhood of the center frequency and increase at the edges of the approximation band. The numerical optimization procedures [38], [39], [40] have results that are much closer to the minimax approximation than the others. This is to be expected because they start with similar approximation criteria.

In all cases in Fig. 14 the $\Delta\varphi_{\max}$ values in brackets confirm that, compared to the other methods, the minimax approximation performs better over the same bandwidth and with the same order.

VII. A PRACTICAL REALIZATION OF FO CAPACITORS AND FO INDUCTORS

In this section the results of the simulations and practical verification from above are presented for the design of real FO capacitors (FOCs) and FO inductors (FOIs). The minimax approximation procedure described in section III is applied to their realization, and the final circuits are compared to the FOC and FOI realizations obtained by the genetic algorithm (GA) in [40] while implemented with commercial components. The corresponding circuits are all designed for the same angle, approximation bandwidth, component number and topology. Since the commercial components are used to replace ideal components, it is expected that the characteristics of the realized circuits will be deteriorated.

A. FO CAPACITORS

For the FOC design using the minimax approximation, the following initial parameters are chosen: $\alpha = -2/3$ ($\varphi_i = -60°$), BW = 10^5 (100Hz-10MHz) and the approximation order $n = 11$. It is compared to the realization given in section III A in [40]. For this purpose, we tried to create the same conditions and use the same tools for the analyses and measurements as in [40].

Using (23) and (24) the impedance function is derived as (43), as shown at the bottom of the next page.

The resulting phase deviation is $\Delta\varphi = \pm 1.4979°$. This impedance function is realized as a Foster 2nd form circuit using the PFE of its reciprocal e.g. the admittance function. The component values are denormalized to $\omega_0 = 1.987 \cdot 10^5$ [rad/s] and $R_0 = 86.6 \cdot 10^6$ [Ω] and shown in the first column of Table 7. The second column contains the nearest commercial component values for the minimax method, and in the third column the commercial components of the circuit realized by the GA procedure in [40] are given. The implemented resistors are taken from the Vishay E96 series 1% 0603 components [70] and the capacitors from the Kemet E24 series 0603 components, or have other nominal values according to their data sheets [71]. Note that in the second column *we use a parallel connection of two capacitors, which is a common design practice*.[9] The phase response of a minimax and GA circuit with nominal commercial element values and tolerances is simulated using OrCAD PSpice; the result is shown in Fig. 15(a). As can be seen, the phase response of the minimax circuit has a maximum phase deviation $\Delta\varphi = \pm 1.5692°$. The maximum phase deviation of the GA circuit is $\Delta\varphi = \pm 2.1°$ in the reduced frequency range 100 Hz - 5 MHz and in the full frequency range 100 Hz - 10 MHz it exceeds the values ±3° [40]. The minimax circuit is further tested by the Monte Carlo simulation in OrCAD PSpice with the histogram

[9]When the difference between the calculated component value and the closest available commercial component value exceeds the tolerated error, a single component is usually replaced by a corresponding serial or parallel connection of two components.

$$Z_{FPA}(s) = \frac{0.019s^6 + 20.17s^5 + 1086s^4 + 4033s^3 + 1059s^2 + 19.2s + 0.017}{s^6 + 217.6s^5 + 3056s^4 + 3021s^3 + 209.8s^2 + 0.943s} \quad (40i)$$

$$Z_{CS}(s) = \frac{0.019s^6 + 20.6s^5 + 1114s^4 + 4289s^3 + 1188s^2 + 22.8s + 0.022}{s^6 + 218.3s^5 + 3171s^4 + 3293s^3 + 239.6s^2 + 1.165s} \quad (40j)$$

TABLE 7. Component values of FOC using the Foster 2nd-form RC network.

Component R [Ω] C [F]	α=−2/3; C_α=3.96 [nF s$^{-1/3}$]		
	Minimax ideal	Minimax commercial	GA in [40] commercial
R_0	11.86 M	11.8 M	10 M
R_1	25.24 k	25.5 k	24 k
R_2	4.67 k	4.64 k	4.7 k
R_3	120.64 k	121 k	110 k
R_4	2.665 M	2.67 M	2.4 M
R_5	575.83 k	576 k	470 k
C_0	5.44 p	5.4 p	7 p
C_1	15.71 p	13p + 2.7p *	18 p
C_2	7.78 p	7.8 p	10 p
C_3	34.32 p	33p + 1.3p *	39 p
C_4	172.65 p	150p + 22p *	200 p
C_5	75.05 p	75 p	91 p
	Operating frequency range		
	100 Hz – 10 MHz		
	Total resistance (MΩ) / Total capacitance (pF)		
	15.26/310.9	15.20/310.2	13.01/365
	Spread of resistance / capacitance Note: *Capacitors in parallel		
	2540.65/31.72	2543.1/31.86	416.67/28.57
	Max. phase deviation (°) Note: **100Hz–5MHz		
	±1.4979	±1.5692	±2.1**
	Monte Carlo analysis: phase variation @ 30kHz (mean / min / max (°))		
	−60.22 / −62.92 / −57.45	−60.14 / −62.83 / −57.58	−60.08 / −62.93 / −57.39

(yield at 30kHz) for the commercial components in Table 7. To investigate the sensitivity of the FOC phase characteristic to the deviation of passive component values, we assume a Gaussian distribution with a zero mean value and the resistors and capacitors as uncorrelated random variables.

After 1500 runs with 1% resistor tolerance and 5% for capacitors, the result is shown in Fig. 15(b) and the corresponding histogram in Fig. 15(c). The mean value with a standard deviation of 0.792629 is −60.1424°, which is very close to the theoretical value −60°. This shows that the realized FOC has a low sensitivity of its phase response to passive components. The Monte Carlo (MC) analysis also confirms that the minimax network achieves the desired phase with higher accuracy when compared to GA, as shown in Table 7.

As a final check, the derived circuit was realized as an RC-breadboard using commercial resistors [70], and capacitors [71], as shown in Fig. 16(a). The phase response is measured in the range 100Hz to 10MHz using the Agilent 4294A precision impedance analyzer. The calibration of the test fixture Agilent 16047E measuring equipment was performed using open circuit, short circuit, and a 100Ω resistor Agilent 04294-61001. The parasitic capacitances influence the circuit at high frequencies and are compensated for by reducing the value of the capacitor C_0 by 1.5pF. The measurement results shown in Fig. 16(b) confirm the higher accuracy of the minimax method: from 100Hz to 10MHz the difference between the markers 0 and 3 is 3.6314° or $\Delta\varphi = \pm 1.8157°$ which is close to the PSpice simulation shown above. Thus, the minimax measurement result is more accurate than the $\Delta\varphi = \pm 2.1°$ obtained by the GA in [40] in the reduced frequency range 100 Hz - 5 MHz, and $\Delta\varphi = \pm 3.2°$ in the full frequency range 100 Hz - 10 MHz.

B. FO INDUCTORS

The initial parameters for the design of the FOI impedance function using the minimax approximation are $\alpha = 1/2$ ($\varphi_i = 45°$), BW $= 10^3$ (10 kHz-10 MHz) and $n = 11$. Using (23) and (24) from the design procedure in section III, the derived normalized impedance is (44), as shown at the bottom of the next page, and the maximum phase deviation $\Delta\varphi = \pm 0.1647345°$. It is also realized as a Foster 2nd-form network shown in Table 8 with the elements denormalized to $\omega_0 = 1.987 \cdot 10^6$ [rad/s] and $R_0 = 1.17646$ [Ω] listed in the first column. The corresponding commercial component values with resistors from Vishay [70] and 0603 E24 series inductors from Coilcraft [72], both with nominal values, are given in the column next to it. Some inductor values are realized as a *parallel connection of two commercial inductors* to achieve closer values to the calculated ones. In the last column the components of the same manufacturer of the GA circuit with the values from [40] are listed. The phase response of both the minimax and GA circuit is simulated with OrCAD PSpice and shown in Figure 17(a). As can be seen in Fig. 17(a), and in Table 8 the phase response obtained by the minimax realization has smaller phase deviations $\Delta\varphi = \pm 0.4016°$ than the GA algorithm with $\Delta\varphi = \pm 1.66°$ in [40]. Using the same simulation parameters as for the RC network case, the Monte Carlo simulation results for the minimax RL network are listed in Table 8 confirming better accuracy than those of the RL network in [40].

$$Z_{Mmx_d}(s) = \frac{0.018s^6 + 20.8s^5 + 1181s^4 + 4515s^3 + 1181s^2 + 20.8s + 0.018}{s^6 + 231.7s^5 + 3396s^4 + 3396s^3 + 231.7s^2 + s} \tag{41d}$$

$$Z_{Mmx}(s) = \frac{10.68s^5 + 1629s^4 + 20938s^3 + 25460s^2 + 2933s + 29.06}{s^6 + 397s^5 + 11332s^4 + 30184s^3 + 7649s^2 + 177s + 0.2121} \tag{43}$$

TABLE 8. Passive element values for FOI using the Foster 2nd-form RL network.

Component R [Ω] L [H]	α=1/2; L_α=834.62 [μH s$^{-1/2}$] 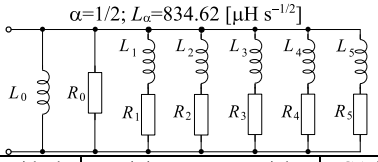		
	Minimax ideal	Minimax commercial	GA in [40] commercial
R_0	16.18	16.2	15
R_1	1.141	1.13	1
R_2	9.389	9.31	10
R_3	0.41212	0.402	1
R_4	2.4552	2.43	1.2
R_5	5.181	5.23	3.9
L_0	8.143 μ	8.2μ (3.6)	6.8 μ
L_1	2.6075 μ	3.3μ (1.5) || 12μ (1.2) *	6.8 μ
L_2	207.41 n	210n (2.06)	220 n
L_3	4.7252 μ	4.7μ (2.1)	6.8 μ
L_4	1.2356 μ	3.9μ (1.6) || 1.8μ (1.1) *	1.2 μ
L_5	574.22 n	580n (0.46)	470 n
	Operating frequency range		
	10 kHz – 10 MHz		
	Total resistance (Ω) / Total inductance (H)		
	34.7583 / 17.493μ	34.702 / 16.72μ	32.1 / 22.29μ
	Spread of resistance / inductance Note: *Inductors in parallel		
	39.26/39.26	40.29/39.05	15/30.91
	Max. phase deviation (°) Note: **12 kHz–10MHz		
	±0.16473	±0.4016	±1.66**
	Monte Carlo analysis: phase variation @ 3 MHz (mean / min / max (°))		
	45.0046 / 43.27 / 46.55	45.1033 / 43.3574 / 46.4703	45.2 / 43.79 / 56.71

The realized breadboard with a Foster 2nd-form RL circuit is shown in Fig. 17(b), and the phase measurement result shown in Fig. 17(c). In the realization of RL networks care must be taken of the problems that arise as a consequence of the parasitic serial resistances of the inductors influencing the frequency response, mainly at low frequencies. Their maximum values given by the manufacturer in the data sheet [72] are shown in the brackets next to the inductance values. In this particular case the problem can be reduced by reducing the values of the serial resistance connected to the inductors by the value of the parasitic resistance. In our RL circuit design we reduced R_3 to 0Ω and R_1 to 0.402Ω. In Fig. 17(c) the difference between the markers 0 and 1 is 8.3924°, e.g. the maximum phase deviation within the frequency band of *two decades* (100kHz - 10MHz) is $\Delta\varphi = \pm 4.1962°$. The GA measurement results in [40] show a maximum phase deviation of $\Delta\varphi = \pm 5.82°$ over the two decades (400kHz - 40MHz). The measurement results confirm that a physical minimax RL network is more accurate than a physical GA RL network.

TABLE 9. Improvement obtained with minimax model in recent applications.

Example of FOE application	$\Delta\varphi$	α	N	BW [decades]
Two FO controllers [5] (2020)	Oustaloup: ±5° **Minimax**: ±2.5°	+1/2	5	5
	Valsa: ±1° **Minimax**: ±0.56°	−0.7	6	3 4
Complex Chebyshev FO filter [12] (2018)	Valsa: ±1° **Minimax**: ±0.3°	−0.7	7	5
	Valsa: ±0.4° **Minimax**: ±0.115°	−0.9	7	5
FOC in FO buck–boost converter [24] (2020)	Oustaloup: ±0.35° **Minimax**: ±0.0044°	−0.95	8	4
FOC in FO buck converter [25] (2019)	Oustaloup: ±3° **Minimax**: ±0.133°	−0.9	7 6	4

C. USING THE MINIMAX MODEL IN RECENT APPLICATIONS

In recent publications [5], [12], [24], [25], researchers designed FOC and FOI elements using physical RC or RL networks to perform measurements in laboratory setups. We have designed the same networks with the same specifications using the minimax approach and found that this results in more accurate networks with a lower number of components. In what follows we compare our minimax approach with that of these authors.

In the two-controller design in [5], the authors use the rational function of Oustaloup and the Valsa RC network. Replacing them by the minimax approximation, the phase error $\Delta\varphi = \pm 5°$ of the first design (Oustaloup) can be improved to ±2.5° (with the same fractional order $\alpha = +1/2$, function order $n = 10$ and BW = 5 decades). For the second (Valsa RC), the phase error $\Delta\varphi = \pm 1°$ and BW = 3 decades (1.7mHz to 1.7Hz) can be improved to an even lower phase error of ±0.56° for BW = 4 decades (1mHz to 10Hz) (with the same fractional order $\alpha = -0.7$ and five Valsa branches, i.e. $n = 11$).

In [12] two seventh-order networks are described using the Valsa procedure for a complex Chebyshev FO low-pass filter with $\alpha = 0.7(63°)$ (with phase error $\Delta\varphi = \pm 1°$) and 0.9 (81°) ($\Delta\varphi = \pm 0.4°$) for a FOC realization within 5 frequency decades. The high sensitivity of the filter performance for the accuracy of the fractional order α is critical. With our minimax approximation, and the same networks but with different component values, we improved the phase errors of $\Delta\varphi = \pm 1°$ to ±0.3° for order 0.7, and of $\Delta\varphi = \pm 0.4°$ to ±0.115° for order 0.9, all within the same BW (100Hz to 10MHz).

In [24] Fang and Wang designed a FO capacitor of order 0.95 (85.5°), using Oustaloup's eighth-order network and obtained a maximum error $\Delta\varphi = \pm 0.35°$ in the frequency

$$Z_{Mmx}(s) = \frac{13.75s^6 + 393.2s^5 + 1902s^4 + 1902s^3 + 393.2s^2 + 13.75s}{s^6 + 94.47s^5 + 1055s^4 + 2303s^3 + 1055s^2 + 94.47s + 1} \tag{44}$$

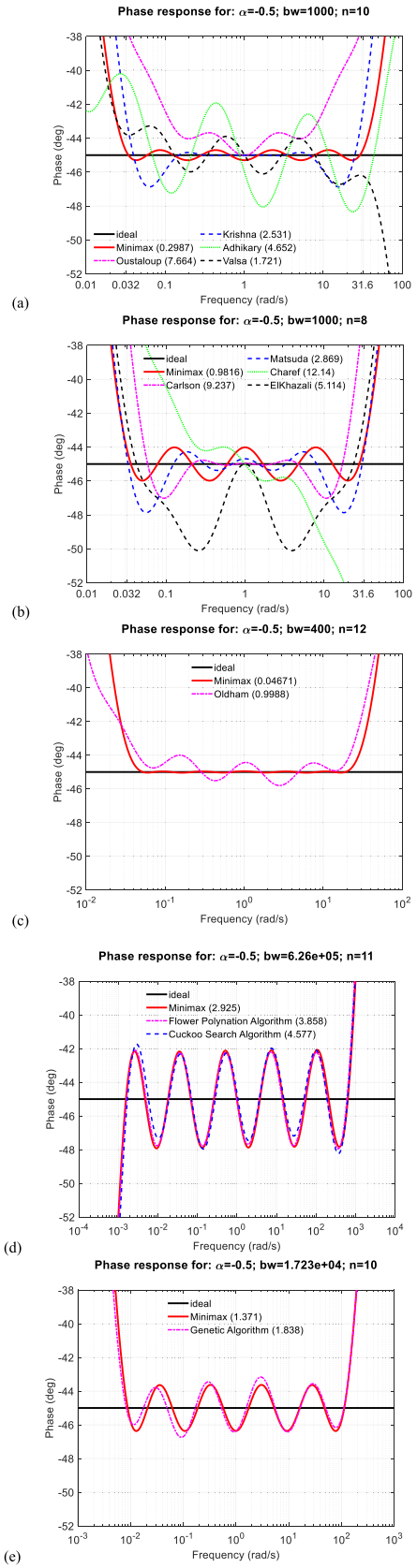

FIGURE 14. Comparison of the minimax function phase (red solid line) to the referenced approximations of the constant phase $\varphi_i = -45°$.

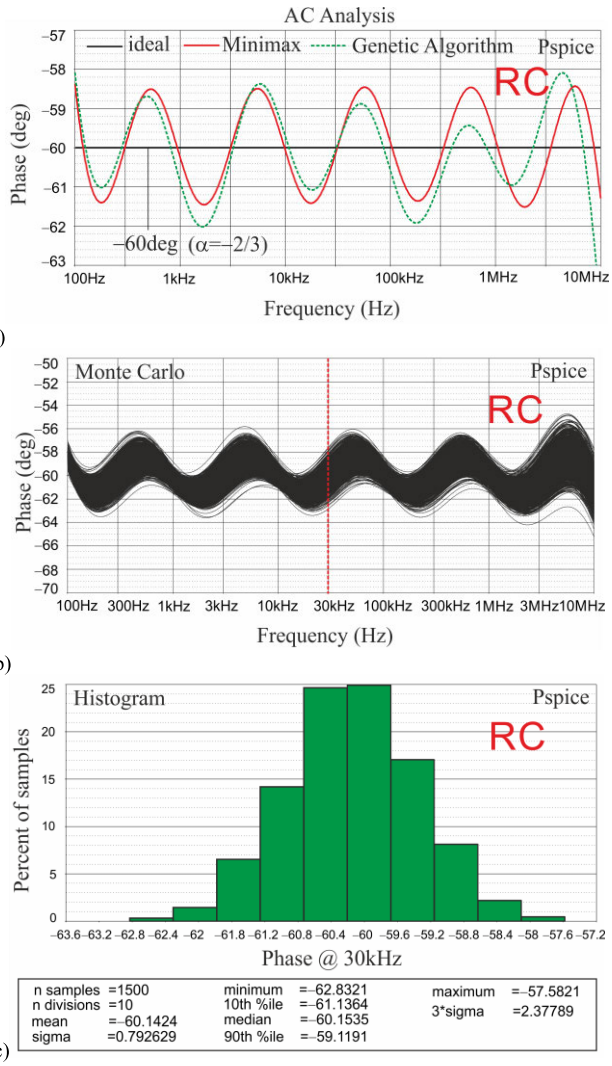

FIGURE 15. (a) Orcad PSpice AC Analysis using the commercial values in the Table 7 derived using GA and minimax algorithms to realize $\varphi_i = -60°$ phase RC network. (b) Monte Carlo (MC) Analysis of minimax RC network for 1500 runs (with 1% for resistors and 5% tolerances for capacitors) (c) Histogram of phase at center frequency 30kHz.

range from 3Hz to 10kHz. With our minimax approximation, we obtained an eighth-order network with the same topology and the same bandwidth, but with a reduced error of $\Delta\varphi = \pm 0.0044°$.

In [25] Wei *et al.* designed an FO capacitor of order 0.9 (81°) using Oustaloup's rational approximation method [52] in the range from 10Hz to 100kHz (4 decades) with a seventh-order physical network and produced a maximum error of $\Delta\varphi = \pm 3°$. With our approach we designed a minimax approximation of the FO capacitor for 4 decades with the same error specifications and obtained a sixth-order network with an error of $\Delta\varphi = \pm 0.133°$.

A comparison of these different design approaches is summarized in Table 9.

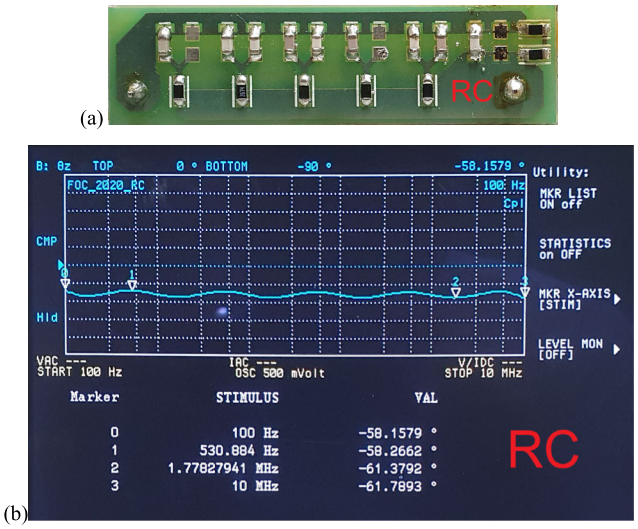

FIGURE 16. (a) The physical SMD realization of FO Capacitor (RC network) RECTANGLE (36 × 10mm) to realize $\varphi_i = -60°$, and (b) phase measurement results on Agilent 4294A precision impedance analyzer with markers.

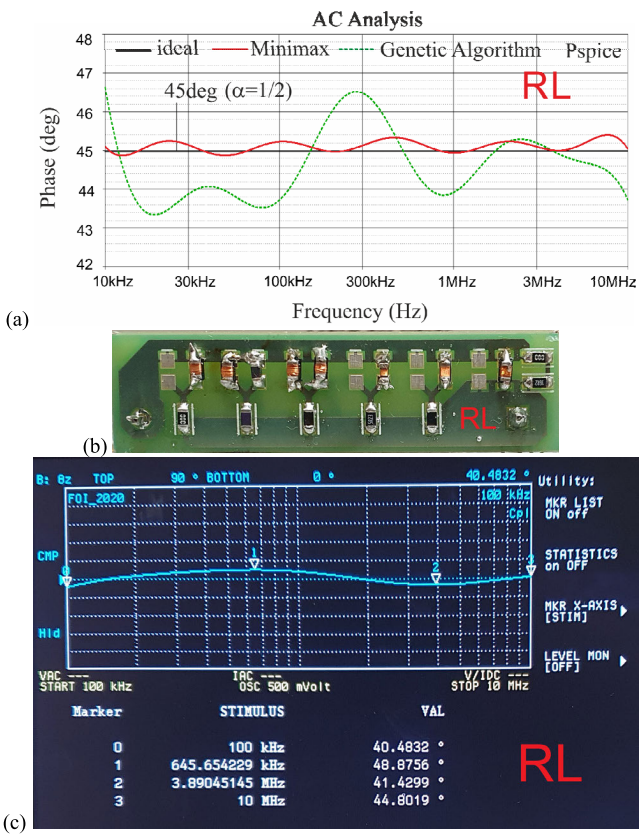

FIGURE 17. (a) Orcad PSpice AC Analysis using the commercial values in the Table 7 derived using GA and minimax algorithms to realize $\varphi_i = +45°$ phase RL network. (b) Rectangle physical SMD realizations of FO Inductor (RL network) and (c) phase measurement results on Agilent 4294A precision impedance analyzer with markers.

D. A MATLAB PROGRAM FOR THE DESIGN OF MINIMAX APPROXIMATED CPEs

A new MATLAB program has been developed for the minimax equiripple phase design of CPEs by physical networks (both passive and active). It is available in [73]. Compared to the only two other available programs [74], [75], it results in more accurate approximations. The first, [74], provides only the Oustaloup transfer function (which is of only odd order). The second, [75], provides only the element values of passive Foster 1 and 2, and Cauer 1 and 2, networks, which are based on Oustaloup, Continued Fraction Expansion (CFE), and Valsa algorithms. Ours is the only program that calculates CPEs based on the minimax approximation. It provides the poles and zeros, transfer function, and complement transfer function, and also calculates the element values of the passive Foster 1 and 2, and Cauer 1 and 2, networks. It provides both RC and RL networks. All the examples in this paper are calculated using this program. With its improved performance compared to the other programs, it may help to fuel the wide-spread use of the minimax approximation in the design of physical, as well as computer simulation model of CPEs. Being simple and comprehensive, it does not need any additional MATLAB toolbox.

VIII. CONCLUSION

In this paper we presented a step-by-step procedure for the realization of basic one-port and two-port FO elements. The procedure involves the approximation of an ideal FO system function $F_i(s) = F_o \cdot s^{\alpha}$ for all possible orders α within the limits $-1 < \alpha < 1$ by standard circuit theory methods. It is based on the "maximally flat" and "minimax" approximation of a constant phase response in the frequency domain. The result is an integer-order rational system function $F(s)$ which approximates $F_i(s)$ in the specified frequency range with a phase error which is within specified limits. Both the frequency band and the phase variations can be specified in advance, and realized at the cost of the system function order, e.g. the final circuit complexity. The "minimax" approximation is chosen for our realization because of its superior properties compared to "maximally flat" and other known approximation methods. The function $F(s)$ can be realized as a one-port or two-port RC or RL circuit. For convenience, we use RC circuits that can realize a basic one-port FOE with α in the range $-1 < \alpha < 0$ and a basic two-port FO model with α in the range $-1 < \alpha < 1$. Using two basic realization procedures, e.g. the Foster and the Cauer methods, *eight* different basic one-port RC circuits for each specific value of fractional-order α are described. The number of circuits can be increased by combining the two methods of circuit realization. Some of the presented basic one-ports are used for the realization of simple FO two-port circuits, such as for FO voltage-mode and current-mode differentiators and integrators.

In order to verify the minimax approximation for FOE design, it is compared to the most frequently referenced approximations obtained by analytical procedures and numerical optimization methods. It is shown that the minimax approximation is generally superior to the ones obtained by analytical methods. The minimax approximation uses two of the three initial parameters for the design e.g., the frequency

bandwidth, the phase deviation, and the approximation order. It calculates the third parameter, and the system function with a magnitude normalized to unity at the center of the normalized frequency bandwidth. All approximation parameters are clearly defined and controlled, which is not the case in many other approximations. We consider its application to fractional-order systems as a novelty because in spite of its excellent properties in many other applications, it was neglected in this field. So far this is the only approximation that takes all relevant approximation parameters into consideration and gives explicit and exact results for a FO system function. The results of numerical optimization methods are mainly close to a minimax approximation, but they are less accurate when the frequency range limits are considered.

The design and simulation results are further verified by the practical realization of an FO capacitor and inductor. They are compared to similar realizations of a recently published method in which FOE components are calculated directly using Genetic Algorithm (GA) design. The analysis performed, and the measurement results obtained, confirm the advantages of the minimax approximation when the accuracy and controllability of all approximation parameters are considered.

The application of the minimax approximation has outperformed the other published approximations used in recent practical applications. The new MATLAB program for the calculations of minimax CPEs is provided on-line and is therefore readily available for the widespread application of the minimax approach to FOE design.

REFERENCES

[1] M. D. Ortigueira, "An introduction to the fractional continuous-time linear systems: The 21st century systems," *IEEE Circuits Syst. Mag.*, vol. 8, no. 3, pp. 19–26, Sep. 2008.

[2] A. S. Elwakil, "Fractional-order circuits and systems: An emerging interdisciplinary research area," *IEEE Circuits Syst. Mag.*, vol. 10, no. 4, pp. 40–50, Nov. 2010.

[3] I. Podlubny, "Fractional-order systems and fractional-order controllers," *Inst. Exp. Phys., Slovak Acad. Sci., Kosice*, vol. 12, no. 3, pp. 1–18, 1994.

[4] I. Dimeas, I. Petras, and C. Psychalinos, "New analog implementation technique for fractional-order controller: A DC motor control," *AEU-Int. J. Electron. Commun.*, vol. 78, pp. 192–200, Aug. 2017.

[5] S. Kapoulea, V. Bizonis, P. Bertsias, C. Psychalinos, A. Elwakil, and I. Petráš, "Reduced active components count electronically adjustable fractional-order controllers: Two design examples," *Electronics*, vol. 9, no. 1, p. 63, Jan. 2020.

[6] A. Charef, "Analogue realisation of fractional-order integrator, differentiator and fractional PIλDμ controller," *IEE Proc.-Control Theory Appl.*, vol. 153, no. 6, pp. 714–720, Nov. 2006.

[7] G. Maione, "Design of cascaded and shifted fractional-order lead compensators for plants with monotonically increasing lags," *Fractal Fract.*, vol. 4, no. 3, pp. 1–20, 2020.

[8] S. Kapoulea, G. Tsirimokou, C. Psychalinos, and A. S. Elwakil, "Employment of the Padé approximation for implementing fractional-order lead/lag compensators," *AEU-Int. J. Electron. Commun.*, vol. 120, Jun. 2020, Art. no. 153203.

[9] K. Baxevanaki, S. Kapoulea, C. Psychalinos, and A. S. Elwakil, "Electronically tunable fractional-order highpass filter for phantom electroencephalographic system model implementation," *AEU-Int. J. Electron. Commun.*, vol. 110, Oct. 2019, Art. no. 152850.

[10] M. C. Tripathy, D. Mondal, K. Biswas, and S. Sen, "Design and performance study of phase-locked loop using fractional-order loop filter," *Int. J. Circuit Theory Appl.*, vol. 43, no. 6, pp. 776–792, Jun. 2015.

[11] R. Verma, N. Pandey, and R. Pandey, "CFOA based low pass and high pass fractional step filter realizations," *AEU-Int. J. Electron. Commun.*, vol. 99, pp. 161–176, Feb. 2019.

[12] A. M. Abdelaty, A. Soltan, W. A. Ahmed, and A. G. Radwan, "On the analysis and design of fractional-order Chebyshev complex filter," *Circuits, Syst., Signal Process.*, vol. 37, no. 3, pp. 915–938, Mar. 2018.

[13] J. Baranowski, M. Pauluk, and A. Tutaj, "Analog realization of fractional filters: Laguerre approximation approach," *AEU-Int. J. Electron. Commun.*, vol. 81, pp. 1–11, Nov. 2017.

[14] D. Jurisic and B. Lutovac, "Third-order fractional-step band-pass filters," in *Proc. 9th Medit. Conf. Embedded Comput. (MECO)*, Jun. 2020, pp. 1–6.

[15] A. Coza, V. Zupanovic, D. Vlah, and D. Jurisic, "Group delay of fractional n+α-order Bessel filters," in *Proc. 43rd Int. Conv. Inf., Commun. Electron. Technol. (MIPRO)*, Sep. 2020, pp. 163–168.

[16] M. C. Tripathy, D. Mondal, K. Biswas, and S. Sen, "Experimental studies on realization of fractional inductors and fractional-order bandpass filters," *Int. J. Circuit Theory Appl.*, vol. 43, no. 9, pp. 1183–1196, 2015.

[17] A. S. Elwakil, A. Allagui, B. J. Maundy, and C. Psychalinos, "A low frequency oscillator using a super-capacitor," *AEU-Int. J. Electron. Commun.*, vol. 70, no. 7, pp. 970–973, Jul. 2016.

[18] G. Tsirimokou, C. Psychalinos, A. S. Elwakil, and K. N. Salama, "Electronically tunable fully integrated fractional-order resonator," *IEEE Trans. Circuits Syst. II, Exp. Briefs*, vol. 65, no. 2, pp. 166–170, Feb. 2018.

[19] G. Tsirimokou, C. Psychalinos, and A. S. Elwakil, "Fractional-order electronically controlled generalized filters," *Int. J. Circuit Theory Appl.*, vol. 45, no. 5, pp. 595–612, May 2017.

[20] S. Westerlund and L. Ekstam, "Capacitor theory," *IEEE Trans. Dielectr. Electr. Insul.*, vol. 1, no. 5, pp. 970–973, Oct. 1994.

[21] S. Westerlund, "Dead matter has memory!" *Phys. Scripta*, vol. 43, no. 2, pp. 174–179, Feb. 1991.

[22] R. Prasad, K. Kothari, and U. Mehta, "Flexible fractional supercapacitor model analyzed in time domain," *IEEE Access*, vol. 7, pp. 122626–122633, 2019.

[23] G. Tsirimokou, C. Psychalinos, A. Allagui, and A. S. Elwakil, "Simple non-impedance-based measuring technique for supercapacitors," *Electron. Lett.*, vol. 51, no. 21, pp. 1699–1701, Oct. 2015.

[24] S. Fang and X. Wang, "Modeling and analysis method of fractional-order buck-boost converter," *Int. J. Circuit Theory Appl.*, vol. 48, no. 9, pp. 1493–1510, Sep. 2020.

[25] Z. Wei, B. Zhang, and Y. Jiang, "Analysis and modeling of fractional-order buck converter based on Riemann–Liouville derivative," *IEEE Access*, vol. 7, pp. 162768–162777, 2019.

[26] B. T. Krishna, "Studies on fractional order differentiators and integrators: A survey," *Signal Process.*, vol. 91, no. 3, pp. 386–426, Mar. 2011.

[27] M. C. Boskovic, T. B. Sekara, B. Lutovac, M. Dakovic, P. D. Mandic, and M. P. Lazarevic, "Analysis of electrical circuits including fractional order elements," in *Proc. 6th Medit. Conf. Embedded Comput. (MECO)*, Jun. 2017, pp. 1–6.

[28] S. V. Shastri and K. S. Narendra, "Fractional order derivatives in systems theory," in *Proc. Amer. Control Conf. (ACC)*, Jul. 2020, pp. 5076–5081.

[29] A. L. Dalcastagne and S. N. Filho, "On the analog generation of pink noise from white noise," in *Proc. IEEE Int. Symp. Circuits Syst.*, no. 4, May 2005, pp. 1944–1947.

[30] D. B. Keele, "The design and use of a simple pseudo random pink-noise generator," *J. Audio Eng. Soc.*, vol. 21, no. 1, pp. 33–41, 1973.

[31] A. Adhikary, M. Khanra, J. Pal, and K. Biswas, "Realization of fractional order elements," *INAE Lett.*, vol. 2, no. 2, pp. 41–47, Jun. 2017.

[32] A. Kartci, N. Herencsar, J. T. Machado, and L. Brancik, "History and progress of fractional-order element passive emulators: A review," *Radioengineering*, vol. 29, no. 2, pp. 296–304, Jun. 2020.

[33] Z. M. Shah, M. Y. Kathjoo, F. A. Khanday, K. Biswas, and C. Psychalinos, "A survey of single and multi-component fractional-order elements (FOEs) and their applications," *Microelectron. J.*, vol. 84, pp. 9–25, Feb. 2019.

[34] A. Adhikary, A. Shil, and K. Biswas, "Realization of Foster structure-based ladder fractor with phase band specification," *Circuits, Syst., Signal Process.*, vol. 39, no. 5, pp. 2272–2292, May 2020.

[35] A. Adhikary, P. Sen, S. Sen, and K. Biswas, "Design and performance study of dynamic fractors in any of the four quadrants," *Circuits, Syst., Signal Process.*, vol. 35, no. 6, pp. 1909–1932, Jun. 2016.

[36] G. Tsirimokou, "A systematic procedure for deriving RC networks of fractional-order elements emulators using MATLAB," *AEU-Int. J. Electron. Commun.*, vol. 78, pp. 7–14, Aug. 2017.
[37] A. Adhikary, S. Choudhary, and S. Sen, "Optimal design for realizing a grounded fractional order inductor using GIC," *IEEE Trans. Circuits Syst. I, Reg. Papers*, vol. 65, no. 8, pp. 2411–2421, Aug. 2018.
[38] A. M. AbdelAty, A. S. Elwakil, A. G. Radwan, C. Psychalinos, and B. J. Maundy, "Approximation of the fractional-order Laplacian s^{α} as a weighted sum of first-order high-pass filters," *IEEE Trans. Circuits Syst. II, Exp. Briefs*, vol. 65, no. 8, pp. 1114–1118, Aug. 2018.
[39] D. Yousri, A. M. Abdelaty, A. G. Radwan, A. S. Elwakil, and C. Psychalinos, "Comprehensive comparison based on meta-heuristic algorithms for approximation of the fractional-order Laplacian s as a weighted sum of first-order high-pass filters," *Microelectron. J.*, vol. 87, pp. 110–120, May 2019.
[40] A. Kartci, A. Agambayev, M. Farhat, N. Herencsar, L. Brancik, H. Bagci, and K. N. Salama, "Synthesis and optimization of fractional-order elements using a genetic algorithm," *IEEE Access*, vol. 7, pp. 80233–80246, 2019.
[41] G. Carlson and C. Halijak, "Approximation of fractional capacitors $(1/s)^{1/n}$ by a regular Newton process," *IEEE Trans. Circuit Theory*, vol. CT-11, no. 2, pp. 210–213, Jun. 1964.
[42] J. A. T. Machado, "Discrete-time fractional-order controllers," *Fractional Calculus Appl. Anal.*, vol. 4, no. 1, pp. 47–66, 2001.
[43] J. Valsa and J. Vlach, "RC models of a constant phase element," *Int. J. Circuit Theory Appl.*, vol. 41, no. 1, pp. 59–67, Oct. 2013.
[44] S. Das, *Functional Fractional Calculus*. Berlin, Germany: Springer, 2011.
[45] R. El-Khazali, "On the biquadratic approximation of fractional-order Laplacian operators," *Analog Integr. Circuits Signal Process.*, vol. 82, no. 3, pp. 503–517, Mar. 2015.
[46] B. M. Vinagre, I. Podlubny, A. Hernandez, and V. Feliu, "Some approximations of fractional order operators used in control theory and applications," *Fractional Calculus Appl. Anal.*, vol. 3, no. 3, pp. 945–950, 2000.
[47] K. Steiglitz, "An RC impedance approximant to $s^{-1/2}$," *IEEE Trans. Circuit Theory*, vol. CT-11, no. 1, pp. 160–161, Mar. 1964.
[48] S. D. Roy, "On the realization of a constant-argument immittance or fractional operator," *IEEE Trans. Circuit Theory*, vol. CT-14, no. 3, pp. 264–274, Sep. 1967.
[49] K. B. Oldham and C. G. Zoski, "Analogue instrumentation for processing polarographic data," *J. Electroanal. Chem. Interfacial Electrochem.*, vol. 157, no. 1, pp. 27–51, Oct. 1983.
[50] A. Charef, H. H. Sun, Y. Y. Tsao, and B. Onaral, "Fractal system as represented by singularity function," *IEEE Trans. Autom. Control*, vol. 37, no. 9, pp. 1465–1470, Sep. 1992.
[51] K. Matsuda and H. Fujii, "H(infinity) optimized wave-absorbing control—Analytical and experimental results," *J. Guid., Control, Dyn.*, vol. 16, no. 6, pp. 1146–1153, Nov. 1993.
[52] A. Oustaloup, F. Levron, B. Mathieu, and F. M. Nanot, "Frequency-band complex noninteger differentiator: Characterization and synthesis," *IEEE Trans. Circuits Syst. I, Fundam. Theory Appl.*, vol. 47, no. 1, pp. 25–39, Jan. 2000.
[53] D. Xue, C. Zhao, and Y. Chen, "A modified approximation method of fractional order system," in *Proc. Int. Conf. Mechatronics Autom.*, Jun. 2006, pp. 1043–1048.
[54] B. T. Krishna and K. V. V. S. Reddy, "Active and passive realization of fractance device of order 1/2," *Act. Passive Electron. Compon.*, vol. 2008, no. 2, pp. 1–5, 2008.
[55] H. W. Bode, *Network Analysis and Feedback Amplifier Design*. New York, NY, USA: David Van Nostrand Company, 1945.
[56] W. Saraga, "The design of wide-band phase splitting networks," *Proc. IRE*, vol. 38, no. 7, pp. 754–770, Jul. 1950.
[57] S. Darlington, "Realization of a constant phase difference," *Bell Syst. Tech. J.*, vol. 29, no. 1, pp. 94–104, Jan. 1950.
[58] H. J. Orchard, "Synthesis of wideband two-phase networks," *Wireless Eng.*, vol. 27, pp. 72–81, Mar. 1950.
[59] D. Weaver, "Design of RC wide-band 90-degree phase-difference network," *Proc. IRE*, vol. 42, no. 4, pp. 671–676, Apr. 1954.
[60] W. Albersheim and F. Shirley, "Computation methods for broad-band 90° phase-difference networks," *IEEE Trans. Circuit Theory*, vol. 16, no. 2, pp. 189–196, 1969.
[61] L. Weinberg, *Network Analysis and Synthesis*, 1st ed. New York, NY, USA: McGraw-Hill, 1962.
[62] N. Balabanian and T. Bickart, *Electrical Network Theory*. Hoboken, NJ, USA: Wiley, 1969.
[63] A. Grossman, "Synthesis of tchebycheff parameter symmetrical filters," *Proc. IRE*, vol. 45, no. 4, pp. 454–473, 1957.
[64] H. J. Orchard and A. N. Willson, "Elliptic functions for filter design," *IEEE Trans. Circuits Syst. I, Fundam. Theory Appl.*, vol. 44, no. 4, pp. 273–287, Apr. 1997.
[65] M. Abramowitz and I. A. Stegun, *Handbook of Mathematical Functions: With Formulas, Graphs and Mathematical Tables* (Dover Books on Mathematics). Mineola, NY, USA: Dover, 1965.
[66] J. Koton, D. Kubanek, N. Herencsar, J. Dvorak, and C. Psychalinos, "Designing constant phase elements of complement order," *Anal. Integr. Circuits Signal Process.*, vol. 97, no. 1, pp. 107–114, Oct. 2018.
[67] S. Kapoulea, C. Psychalinos, and A. S. Elwakil, "Minimization of spread of time-constants and scaling factors in fractional-order differentiator and integrator realizations," *Circuits, Syst., Signal Process.*, vol. 37, no. 12, pp. 5647–5663, Dec. 2018.
[68] S. K. Mitra, "A network transformation for active RC networks," *Proc. IEEE*, vol. 55, no. 11, pp. 2021–2022, Nov. 1967.
[69] A. N. Khovanskii, *The Application of Continued Fractions and Their Generalizations to Problems in Approximation Theory*, P. Wynn, Ed. Groningen, The Netherland: P. Noordhoff Ltd., 1963.
[70] *High Frequency 50 GHz Thin Film 0402 Chip Resistor*, document 53014, Datasheet: Vishay Intertechnology Inc., 2018. [Online]. Available: https://www.vishay.com/docs/53014/ch.pdf
[71] *HiQ-CBR Series, 0402 C0G Dielectric, Low ESR 6.3_500 VDC, 1 MHz 50 GHz (RF & Microwave)*, document C1030_C0G_CBR, Datasheet: Kemet Electronics Corporation, 2018. [Online]. Available: https://goo.gl/fdpbQ8
[72] *Magnetics for RF, Power, Filter and Data Applications_0603 Ceramic Inductors*, document 0603LS (1608), Datasheet: Coilcraft, Inc., 2018. [Online]. Available: https://www.coilcraft.com/pdfs/ShortFormCatalog.pdf
[73] D. Jurisic, N. Mijat, and G. Moschytz. (2020). MATLAB code for calculating the minimax immittance for approximating fractional-order elements. MATLAB File Exchange. Accessed: Jul. 8, 2021. [Online]. Available: https://www.mathworks.com/matlabcentral/fileexchange/96762-fractional-order-elements-foes-using-minimax-approximation
[74] Y. Chen. (2003). Oustaloup-recursive-approximation for fractional order differentiator. MATLAB File Exchange. Accessed: Jul. 8, 2021. [Online]. Available: https://www.mathworks.com/matlabcentral/fileexchange/3802-oustaloup-recursive-approximation-for-fractional-order-differentiators
[75] C. Psychalinos and G. Tsirimokou. (2018). MATLAB code for calculating the passive elements values of RC networks used for approximating fractional-order capacitors. Research Gate. Accessed: Jul. 8, 2021. [Online]. Available: https://www.researchgate.net/publication/328768056_Matlab_code_for_calculating_the_passive_elements_values_of_RC_networks_used_for_approximating_fractional-order_capacitors

NEVEN MIJAT (Life Member, IEEE) received the Dipl.-ing., M.Sc., and Ph.D. degrees in electrical engineering from the Faculty of Electrical Engineering, University of Zagreb, in 1970, 1974, and 1984, respectively. In 1970, he joined the Department of Electronic Systems and Information Processing, Faculty of Electrical Engineering. During his professional involvement as a Professor, he led courses and supervised research and development projects and activities involving circuit theory, signal processing, filters, analog circuits, and SC circuits. He was the Principal Investigator for several scientific projects sponsored by the Croatian Ministry of Science and numerous projects for companies. He is a member of CROMBES, KoREMA, and some other professional societies.

DRAZEN JURISIC (Member, IEEE) received the B.Sc., M.Sc., and Ph.D. degrees in electrical engineering from the University of Zagreb, Croatia, in 1990, 1995, and 2002, respectively. He is a Full Professor with the Faculty of Electrical Engineering and Computing (FER), University of Zagreb. He lectures in the field of electrical circuits, signals and systems, and analog and mixed-signal processing circuitry. From 1997 to 1999, he was with the Institute of Signal and Information Processing, Swiss Federal Institute of Technology (ETH), Zürich, Switzerland. Since 2008, he has been visiting the Faculty of Engineering, Bar-Ilan University, Israel, and doing research in the field of analog circuits and filters. His research interests include analog and digital signal processing and filter design, integrated circuit design, and the study and analysis of fractional-order systems. He is currently the MC Member of the COST Action CA15225 "Fractional-order systems—Analysis, synthesis and their importance for future design." He is also a member of the Croatian Society for Communications, Computing, Electronics, Measurement and Control and the IEEE-CAS Society. He was awarded the Silver Plaque Josip Loncar for his Ph.D. thesis and an IEEE Best Paper Finalist Award for a conference paper.

GEORGE S. MOSCHYTZ (Life Fellow, IEEE) received the bachelor's and Ph.D. degrees from the Swiss Federal Institute of Technology (ETH), Zürich, Switzerland. He is the Founder and was the Dean of the School of Engineering (Electrical, Computer, and Bio-Engineering), Bar-Ilan University, Israel (founded in 2001). He was also a Professor and the Director of the Institute for Signal and Information Processing, Swiss Federal Institute of Technology (ETH), from 1973 to 2001. Before he joined the EE Department, ETH, he was at RCA Research Laboratories, Zürich, and then for close to ten years, at Bell Telephone Laboratories, New Jersey, USA. At Bell Laboratories, he supervised a group designing analog and digital integrated circuits and filters for data communications. He has written and coauthored several books on analog, digital, switched capacitor, and adaptive circuit and filter design, and over 400 articles in the field of network theory and design, signal processing, and circuit sensitivity. He holds a number of patents in these areas. He was awarded the IEEE-CAS-Education Award, and the IEEE-CAS Mac Van Valkenburg Award, as well as several other IEEE awards (among them the Golden Jubilee Award and the Third Millennium Medal). He was the President of the IEEE Circuits and Systems Society in 1999. While at ETH, he served for the ETH Research Council, then for the Swiss National Research Council, Berne, and, thereafter, was one of the two representatives of Switzerland for the European Research Council, Brussels.